Synergistic *MAPT* mutations as a platform to uncover modifiers of tau pathogenesis

Miles R. Bryan III[1,2], Michael F. Almeida[2,3,4], Kyle Pellegrino[1,4], Carli K. Opland[1], Ethan Paulakonis, J.[1] Jake McGillion-Moore[1], Hanna Trzeciakiewicz[1], Diamond King[1], Xu Tian[1], Jui-Heng Tseng[1,2,5], Jonathan C. Schisler[3,4], Nicholas G. Brown[4], Ben A. Bahr[2,6], Todd J. Cohen[1,2*]

[1]Neurology, University of North Carolina- Chapel Hill, NC
[2]Duke-University of North Carolina Alzheimer's Disease Research Center (ADRC), 2424 Erwin Road, Durham, North Carolina 27705
[3]McAllister Heart Institute and the Department of Pharmacology, 111 Mason Farm Road, University of North Carolina - Chapel Hill, Chapel Hill, North Carolina 27514 U.S.A.
[4]Pharmacology, University of North Carolina- Chapel Hill, NC
[5]School of Life Sciences, Arizona State University- Tempe, AZ
[6]Biotechnology Research and Training Center, University of North Carolina- Pembroke, NC

From the Department of Neurology, UNC Neuroscience Center, University of North Carolina, Chapel Hill North Carolina, 27599

*To whom correspondence should be addressed: Todd J. Cohen: Department of Neurology, University of North Carolina at Chapel Hill, Chapel Hill NC 27599
toddcohen@neurology.unc.edu; Tel. (919) 966-3759; Fax. (919) 843-4576

Keywords*:* aggregation, Alzheimer's disease, FTDP-17, MAPT, posttranslational modification (PTM), heat-shock proteins, Hsp70, organotypic brain slices, neurodegeneration, tau, tauopathy

---

Abstract

The natively unfolded tau (MAPT) protein is extremely soluble, which poses challenges when modeling neurofibrillary tangle (NFT) pathology in Alzheimer's disease (AD). To overcome this hurdle, we combined P301L and S320F mutations (PL-SF) to generate a rapid and reliable tau pathology platform to expedite the discovery of factors that modify tau aggregation. Using this model, we evaluated heat-shock proteins (Hsp), which have been linked to tau pathology, but whose role in AD remains enigmatic and controversial. In primary neurons, expression of Hsp70, but not Hsc70 or Hsp90, exacerbated tau aggregation. Conversely, lowering Hsp70 or employing a chaperone-deficient tau mutant (PL-SF-4Δ) reduced tau phosphorylation and abrogated tau aggregation, highlighting Hsp70 as a key driver of tau aggregation. Hsp70 foci clustered within

and surrounding neuritic plaques and NFTs in post-mortem AD brain. Functionally, mature aggregate-bearing neurons showed deficits in neuronal firing and network communication, which were restored by chaperone-binding deficient tau variants that abrogated tau pathology. This study provides a powerful cell-intrinsic model for accelerated tau aggregation, which can be harnessed to identify potent regulators of tau aggregation as promising therapeutic targets.

Introduction

Aggregation of the microtubule-associated protein tau (MAPT) and the formation of insoluble tau inclusion pathology are hallmark features of Alzheimer's disease and related neurodegenerative disorders. In contrast to AD, in which tau pathology is comprised of normal wild-type tau proteins, pathogenic disease-causing mutations in *MAPT* are implicated in familial frontotemporal dementia linked to chromosome 17 (FTDP-17). Over 50 different pathogenic *MAPT* missense, silent, and intronic mutations have been identified[1]. In many instances, missense mutations generate loss and gain of function phenotypes including altered microtubule (MT) binding and enhanced tau aggregation propensity, which are implicated in prion-like tau spreading along defined spatial and temporal brain networks[2–4].

While familial missense mutations at residue P301 (e.g., P301L and P301S) have been well characterized as aggregate-prone and MT-binding deficient, less is known about nearby mutations within the MT-binding repeat domain (MTBR)[5,6]. Our recent study characterized a panel of FTDP-17 tau mutations spanning this domain and found that the cellular surveillance machinery composed of HDAC6 and associated chaperones (e.g. Hsp70) shows increased binding to two specific mutations within the R3 domain (P301L and S320F), but not others, suggesting these two

34 mutants are conformationally distinct and are more effectively recognized by the quality control
35 machinery that targets tau for degradation[7].

36 In separate studies, the P301L and S320F mutations were combined into the same full-
37 length tau molecule (termed PL-SF), which generated a surprisingly aggregate-prone
38 conformation leading to an accelerated AD-like tangle pathology, neuroinflammation, and
39 memory impairments in mice and rhesus macaques[8–12]. Thus, PL-SF could potentially be
40 leveraged as an intrinsic, cell-autonomous, and seeding-independent model of full-length tau
41 aggregation, which would otherwise be challenging to achieve with full-length tau. In fact, many
42 widely used tau models, including the tau biosensor cell lines, employ artificially truncated tau
43 mutants comprising only the tau repeat domain, a fragment with questionable physiological
44 relevance to neurons[13] . In comparison, the PL-SF model offers several advantages, including
45 serving as a rapid model of full-length and mature tau aggregation as a cornerstone for high-
46 throughput discovery of tau modifiers[8,9,11,14].

47 Among known tau interactors, heat shock proteins (Hsps) such as inducible Hsp70,
48 constitutive Hsc70and related Hsp90 have high affinity for aberrant forms of tau, yet their
49 functions as refolding and/or triaging factors remains unclear[8,9,1516–25]. This debate has obvious
50 therapeutic implications since Hsp inhibitors are in clinical development and have been evaluated
51 in preclinical models of AD[26–31]. However, prior studies have yielded quite contradictory and even
52 opposing results, since on the one hand, Hsp70 is thought to promote the MC1-positive tau
53 conformation[18], while other studies suggest Hsp70 and Hsc70 mediate tau degradation via
54 autophagy and the ubiquitin-proteasome system (UPS)[32,33]. One possible explanation for these
55 discrepancies is the inability to generate mature tau pathology in these studies, as observed in
56 human AD brains. Adding additional complexity, tau interacts with dozens of chaperone adaptors

57 and cofactors that may promote or suppress chaperone function directed towards tau[20,21,34,35]. Here,
58 we characterized a tau PL-SF model of accelerated tau pathology, which allowed us to interrogate
59 the role of Hsp70 and other chaperones as bona fide modifiers of tau-mediated toxicity and
60 aggregation.
61
62 **Results**
63
64 **Synergistic familial *MAPT* mutations drive tau phosphorylation and aggregation**
65 We first evaluated tau aggregation in PL-SF expressing immortalized QBI-293 cells. Cells
66 transfected with human T40 (2N4R) wild-type, P301L, S320F, or PL-SF were monitored for
67 RIPA-soluble expression of phosphorylated tau (AT8 and AT100) and cleaved tau (TauC3), two
68 well-established markers of tau pathogenesis. Phosphorylated tau accumulated in PL-SF
69 expressing cells, more so than WT or either single mutant (**Figure 1 A, B**). Confirming this finding,
70 total tau immunoblotting revealed up-shifted tau protein bands in SF and PL-SF, indicative of tau
71 hyperphosphorylation. Surprisingly, the single PL mutant appeared hypo-phosphorylated
72 compared to WT or SF mutations. Immunocytochemistry confirmed these findings and revealed
73 Thioflavin S (ThioS) positive SF and PL-SF aggregates, consistent with enhanced tau aggregation
74 (**Supplemental Figure 1, Figure 1C**). Similar to phosphorylated tau, cleaved tau also
75 preferentially accumulated in SF or PL-SF expressing cells.
76 Multiple familial FTD-associated mutations occur at residue P301 (P301L, P301S, P301T)
77 and S320 (S320F, S320Y). We evaluated a panel of other combination mutants by immunoblotting
78 and immunocytochemistry and found that all double mutants formed phosphorylated, cleaved, and

insoluble tau species compared to individual single tau mutants (**Supplemental Figure 2**). The most consistently insoluble tau species was PL-SF, which we selected for follow-up analysis.

A prior study found that deletion of four key residues in tau (I277/I278 and I308/V309) can abrogate Hsp70 binding[36]. Since the role of Hsp70 in tau pathology is unclear, we generated a PL-SF mutant in which these four residues were depleted, termed PL-SF 4Δ. In transfected QBI-293 cells, PL-SF 4Δ was nearly completely dephosphorylated and accumulated negligible amounts of cleaved tau. PL-SF 4Δ was also downshifted compared to PL-SF (**Figure 1D, E**) and showed significantly less phosphorylated (AT8), cleaved (TauC3), and aggregated (ThioS) tau (**Supplemental Figure 3, Figure 1F**). By co-immunoprecipitation assays, we confirmed that PL-SF 4Δ abrogated the majority of Hsc70 and Hsp70 binding to tau. We did not observe detectable and specific binding to endogenous Hsp90 in our model (**Figure 1G**).

We also assessed the impact of tau mutants on acetylated-tubulin (ac-tubulin), a readout for microtubule (MT) stability and dynamics. Wild-type tau increased ac-tubulin, as expected, while P301L or S320F were less effective (~30-40%). Consistent with a near-complete loss of MT regulatory function, PL-SF reduced ac-tubulin levels down to the levels of non-transfected cells. Surprisingly, PL-SF 4Δ partly restored the tubulin interactions (**Figure 1H, I**).

To confirm that PL-SF has increased intrinsic propensity to self-aggregate, as opposed to being influenced by other cellular factors, we performed in vitro Thioflavin T (ThioT) assays using recombinant purified tau proteins to assess aggregation kinetics in the presence of heparin as an inducing agent. Indeed, PL-SF tau rapidly aggregated within 1 hr post-induction, at which point the formation of recombinant tau fibrils plateaued, while PL-SF 4Δ was completely resistant to aggregation, even though similar tau concentrations were present (**Figure 1J**).

102 **Impaired chaperone binding alleviates tau pathology in neurons**

103 To validate our findings in neurons, we developed mutant tau lentiviral constructs suitable
104 for high-efficiency transduction into mouse primary cortical neurons. Transduced primary
105 neurons were evaluated with a panel of tau mutants, including PL-SF. Immunoblotting of neuronal
106 lysates showed that PL-SF tau was again up-shifted and accumulated more phosphorylated tau
107 (**Figure 2A, B).** Unlike immortalized cell lines, neurons did not show appreciable levels of cleaved
108 tau (TauC3). Only PL-SF accumulated in the insoluble fraction (**Figure 2C**). PL-SF 4Δ showed a
109 marked reduction in tau phosphorylation and aggregation, suggesting a similar phenotype in
110 neurons as well. In fact, deletion of just two of the Hsp-binding residues (ΔI277/I278 or
111 ΔI308/V309) abrogated tau phosphorylation and aggregation, with residues I308/V309 showing
112 the most dominant effect (**Figure 2A-C**). Introduction of β-sheet disrupting proline mutations has
113 been shown to abrogate tau aggregation[37–41]. Indeed, by mutating residues I277 and I308 to
114 prolines (PL-SF I277P/I308P), we were able to suppress tau aggregation to similar levels as seen
115 in PL-SF 4Δ (**Supplemental Figure 4**).

116 By performing microscopy on transduced neurons, we found that PL-SF accumulated AT8,
117 MC1, and ThioS-positive tau inclusions (**Figure 2D, E**). Both MC1 (pre-tangle confirmational
118 tau) and AT8 immunoreactive tau were amorphous and globular and accumulated as large
119 varicosities, or swellings, within neurites. The large globular tau aggregates colocalized with
120 ThioS, supporting tangle-like pathology (**Figure 2F, G**). By transducing neuronal cultures with
121 GFP-tagged PL-SF and labeling neurons with a mouse-specific tau antibody (monoclonal T49),
122 we observed recruitment of endogenous mouse tau to PL-SF inclusions, implying that no species
123 barrier exists between human PL-SF aggregates and mouse tau (**Figure 2H**). PL-SF behaved

124 similarly in tau knockout neurons, and therefore, endogenous tau is not required for the
125 accumulation of PL-SF pathology in neurons (**Supplemental Figure 5**).
126
127 **Hsp70 promotes tau hyperphosphorylation and aggregation**
128 To determine whether Hsp70 is a more potent regulator of tau pathology compared to other
129 tau-associated heat shock proteins, PL-SF expressing neurons were co-transduced with either
130 HSP70, HSC70, or HSP90. Only Hsp70, but not Hsc70 or Hsp90, exacerbated tau phosphorylation
131 (AT8), which was supported by an appreciable upshift in tau's molecular weight (**Figure 3A, B**)
132 and a trend towards increased levels of total insoluble tau (**Figure 3C, D**). Hsp70 significantly
133 increased AT8, MC1, and ThioS immunoreactivity (**Figure 3E, F**). The effect of Hsp70 appears
134 remarkably specific to the aggregate-prone PL-SF tau, since the P301L single mutant was
135 unaffected **(Supplemental Figure 6).**
136 Next, we depleted HSP70 in PL-SF transduced neurons. We achieved ~ 50% Hsp70
137 knockdown using lentiviral shRNA transduction, which did not affect HSC70 expression.
138 Strikingly, HSP70 knockdown led to ~70% decrease in phosphorylated tau (**Figure 4 A, B**) and
139 ~50% decrease in total insoluble tau (**Figure 4C, D**). We note that a ~50% decrease in soluble tau
140 was also observed, suggesting that Hsp70 depletion enhances the turnover of steady-state tau levels
141 (**Figure 4A, B**). The impact of Hsp70 on tau also appears to be quite specific since knockdown of
142 HSP90 did not alter total or phosphorylated tau (**Supplementary Figure 7**). Overall, our findings
143 highlight Hsp70 as a primary regulator of aggregate-prone tau species in this accelerated PL-SF
144 tau model.
145
146 **Cell-autonomous aggregated tau alters neuronal activity and network synchrony**

147 Given the extensive tau pathology observed in PL-SF transduced neurons, we evaluated
148 any deficits in neuronal activity and connectivity. Electrically active neurons were transduced at
149 DIV18 following an initial multi-electrode array (MEA) recording. Daily recordings were taken
150 for 53 days, and in parallel, neurons were immunolabeled at DIV29 and DIV62 to assess the extent
151 of tau pathology.

152 We evaluated the mean firing rate (a measure of overall activity), the number of network
153 bursts (a measure of neuronal connectivity), and the area under the normalized crossed-correlation
154 (a readout for neuronal synchrony). After 15-20 days post-lentiviral transduction, PL-SF neurons
155 showed a decline in all three metrics, suggesting a loss in neuronal activity and reduced
156 synchronous firing across neuronal networks. The deficits worsened over time, but some neurons
157 continued to fire even past DIV50 (**Figure 5A-C**). Raster plots at DIV54 highlight reduced
158 network firing across electrodes and elongated network firing time (**Figure 5D-F**). PL-SF 4Δ did
159 not exhibit any deficits in any of the activity metrics and showed similar firing patterns as
160 compared to wild-type control neurons (**Figure 5A-C**).

161 The impact of aggregate-prone tau mutants on neuronal firing could represent a direct
162 effect of tau at the synapse. Therefore, we assessed whether PL-SF accumulated at the post-
163 synaptic density (PSD), a re-localization thought to coincide with synaptic dysfunction. PSD
164 fractions were biochemically isolated from transduced neurons at DIV18 and probed by
165 immunoblotting for phosphorylated and total tau. PL-SF accumulated in the PSD fraction, which
166 was not observed with PL-SF 4Δ or any single tau mutants (e.g., P301L) (**Figure 5G**). We
167 conclude that mature PL-SF tau aggregates accumulate at the PSD and drive synaptic dysfunction.
168 By abrogating Hsp binding, PL-SF 4Δ bypasses these defects.

169 PL-SF expressing neurons were aged in culture to determine tau phenotypes over time.
170 Indeed, aged neurons accumulated dense tau inclusions comprised of phosphorylated, MC1, and
171 ThioS-positive tau at DIV29, which became even more intensely labeled by DIV62. All indicators
172 of tau pathology were absent in PL-SF 4Δ expressing neurons, even at late time points (**Figure**
173 **5H**). We also note that Hsp70 began to colocalize with aggregated tau in aged neurons (**Figure**
174 **5I**), supporting aggregation-dependent recruitment of Hsp70.
175

176 **Cell-autonomous tau pathology in organotypic brain slice cultures**

177 To validate our findings in brain culture systems comprised of both neurons and glia, we
178 transduced adult rat organotypic hippocampal brain slices ex vivo with either GFP alone, wild-
179 type tau-GFP, PL-SF-GFP, or PL-SF 4Δ-GFP at DIV1 and imaged brain slices after nine weeks in
180 culture **(Figure 6A, B**). Similar to cultured neurons, PL-SF accumulated dense AT8 and MC1-
181 positive inclusions and distinct neuritic puncta, or foci. Most tau pathology preferentially
182 accumulated in the dentate gyrus (DG) and extended through the hippocampal CA1 and CA3
183 regions. In contrast, PL-SF 4Δ exhibited diffuse, non-aggregated neuronal labeling in the DG and
184 showed far lower levels of pathogenic tau markers, such as MC1 and AT8 **(Figure 6C, D)**. These
185 data suggest that, in a multicellular model with complete hippocampal architecture, abrogating
186 tau-Hsp binding can confer neuroprotection.
187

188 **Hsp70 is upregulated in human AD brain and intercalates within tau aggregates.**

189 Finally, we evaluated Hsp70 levels and localization in AD human post-mortem brain.
190 Biochemical fractionation of control and AD brain lysates showed elevated Hsp70 expression in
191 both soluble (hi-salt extracted) and insoluble (urea extracted) whole cortex AD brain homogenates

192 (**Figure 7A,B**). Hsc70 was only upregulated in the insoluble fraction of AD brains (**Figure 7C,D**).
193 We then performed immunohistochemistry on AD hippocampus and found that the vast majority
194 of AT8-positive tau aggregates (plaques and tangles) were labeled by Hsp70-positive foci (**Figure**
195 **7E, Supplemental Figure 8**). Interestingly, the Hsp70 foci formed discrete puncta that appeared
196 to intercalate within the AT8-positive tau neuritic plaques and neurofibrillary tangles (NFTs). This
197 data further supports a prominent role for Hsp70 in modulating tau accumulation in human AD
198 brain.
199

200 **Discussion**

201 Here, we developed and characterized a cell-autonomous model of tau aggregation based
202 on the synergistic aggregation of tau missense mutations at residues P301 and S320. Given the
203 rapid and robust tau aggregation observed within days (in primary neurons), the PL-SF model
204 readily lends itself to identifying factors that modulate tau aggregation. We leveraged this model
205 to clarify the longstanding debate on the role of Hsp70 as a tau modifier. The PL-SF model could
206 address the stepwise development of tau pathology and provide a more reliable and sensitive
207 system for identifying subtle regulators of tau pathogenesis.
208

209 **Synergistic tau mutants as a model of mature tauopathy**

210 Prior studies have suggested that combining tau mutations at P301 and S320 (e.g. PL-SF)
211 can lead to accelerated tau aggregation[8–11,14], leading to the development of new cell culture and
212 mammalian models that better recapitulate tau pathology. For example, the S320F mutation was
213 introduced in P301S/S305N knock-in mice, resulting in enhanced tau pathology[42]. Recently,
214 AAV-mediated delivery of PL-SF tau to rhesus macaques was able to induce rapid and progressive

215 tau pathology, demonstrating its utility as an efficient primate model for studying AD[43] . Here,
216 we analyzed the biochemical and histological properties of PL-SF in cells, cortical neurons, and
217 organotypic brain slice cultures. Strikingly, PL-SF tau inclusions appear quite similar to those
218 detected in post-mortem AD brain (**Figures 1, 2, 6, 7**). Future cryo-EM studies may be needed to
219 better define their ultrastructural properties[44–47] . However, if PL-SF does indeed form AD-like
220 filaments, it may be a preferred model over other single tau variants (P301S and P301L) that lack
221 mature amyloid structure in culture and mouse models[48,49]. The PL-SF tau variant also
222 accumulated at the post-synaptic density (PSD), leading to functional deficits in neuronal firing
223 and connectivity (**Figure 5 A-H**), which supports its synaptic toxicity. This rapidly maturing
224 pathology likely allows for sensitized functional defects at the synapse.

225 Exactly how these two mutations (P301L or S320F) synergize to promote tau pathology
226 and drive tau-mediated toxicity is unclear. But we can envision several scenarios. First, P301L and
227 P301S have been well-characterized for disrupting MT dynamics and promoting tau aggregation;
228 however, less is known about S320F, which is linked to Pick's disease. Recently, S320F was found
229 to stabilize a hydrophobic pocket of tau, exposing the ^{306}VQIVYK^{311} amyloid motif and thereby
230 promoting aggregation[5]. The combination of these two mutations likely amplifies their proclivity
231 towards β-sheet self-assembly. To further test this, we generated PL-SF I277P/I308P containing
232 two amyloid-breaking proline mutations within the MTBR. Indeed, insertion of β-breaking
233 mutations suppressed tau aggregation in primary neurons (**Supplemental Figure 4**), in line with
234 previous in vitro studies[37–41].

235 Second, by extension of its aggregation propensity, PL-SF tau may also be more highly
236 decorated with pathological PTMs than either single tau mutant, driving conformational changes
237 (i.e., MC1). In this study, we only evaluated well-known tau phosphorylation epitopes (AT8,

238 AT100, AT180), but future mass spectrometry approaches could determine the temporal
239 emergence of global tau PTMs (**Figure 2A, B**). For instance, increased PTM complexity could
240 create a feed-forward cycle leading to further loss of tau-MT binding. One can also envision PTM-
241 induced loss of tau binding to quality control machinery, which typically acts in a compensatory
242 manner to prevent aberrant tau[7]. One example is the surveillance factor HDAC6, which binds and
243 maintains tau in the deacetylated state[7]. Thus, PL-SF could overburden the cellular proteostasis
244 capacity, as suggested for human AD[50–52].

245 Third, P301L and S320F mutations are also known to dissociate tau from microtubules,
246 which would shift and favor their equilibrium, further concentrating tau pools in the cytosol and
247 facilitating their aggregation. PL-SF drastically reduced acetylated-tubulin levels back down to
248 baseline (i.e., non-tau expressing cells) (**Figure 1 H, I**), suggesting PL-SF is almost completely
249 disassociated from microtubules and therefore more readily primed for aggregation.

250 Lastly, once formed, we found that neuronal PL-SF tau can recruit endogenous mouse tau
251 (detected by T49 antibody) into tau inclusions (**Figure 2H**), consistent with a prior study showing
252 that human PL-SF-expressing mice (SPAM mice) recruited endogenous mouse tau[11,14]. PL-SF tau,
253 therefore, may be more highly seeding competent, in a species-independent manner, which could
254 be leveraged to model tau spreading since it poses several advantages over the use of exogenously
255 added, brain-derived AD seeds (e.g., large-scale production, reliability and reproducibility, and
256 fully intact N-terminal domains). We reiterate that further ultrastructural studies are needed to
257 determine whether seeding-competent PL-SF resembles human AD brain-derived tau.

258

259 **The role of Hsp70 in tau pathology**

260 We added clarity to the long-standing question of whether Hsp70 modulates tau
261 aggregation, as the prior literature is inconsistent and often highlights contradictory models for tau
262 triage via coordinated Hsp binding. Some studies have found that activation or overexpression of
263 Hsp70 can suppress tau aggregation in vitro, which would intuitively suggest a classical Hsp70
264 chaperone activity as a suppressor of tau aggregation[17,32,33,53] . Adding additional complexity,
265 while Hsp70 can disassemble tau filaments isolated from human AD brain, this chaperone activity
266 can release seeding-competent tau species, suggesting any protection afforded by Hsp70 may
267 depend on the nature of the chaperone-liberated tau species[54]. In contrast, other studies have shown
268 that Hsp70 depletion or small molecule inhibition (YM-01, JG-23/48) may drive tau
269 clearance[22,23,28,30,55–57]. We sought to reconcile these differences in the context of our PL-SF
270 cellular model of tau aggregation.

271 We initially found that Hsp70 was tightly associated with PL-SF tau aggregates in vitro
272 and in cell culture, a finding consistent with a previous study[58] (**Figure 5I**). HSP70 overexpression
273 was associated with PL-SF phosphorylation and aggregation, while HSP70 depletion reduced total
274 tau levels, including hyperphosphorylated and aggregated tau species (**Figure 3A-D, Figure 4A-**
275 **D**). Furthermore, abrogating Hsp70 binding using an Hsp70-binding deficient mutant (PL-SF-4Δ)
276 was also sufficient to suppress tau aggregation (**Figure 1, 2, 5, 6)**. Further supporting a role for
277 Hsp70 in human AD pathology, we found that Hsp70 is upregulated in AD hippocampus and
278 heavily intercalated within neuritic plaques and NFTs (**Figure 7**). The Hsp70 localization pattern
279 was highly consistent in human AD hippocampus (**Supplemental Figure 8**) and illustrates a
280 unique tau-Hsp70 pattern of co-pathology[59–61]. The lack of complete colocalization suggests that
281 Hsp70 recruitment to tau occurs in a time-dependent manner. At least in a mature tau aggregation

282 model, these data are consistent with Hsp70 stabilizing a misfolded tau conformation that
283 potentially evades proper triage and/or degradation.

284 In addition to Hsp70, tau is also an Hsp90 substrate, which competes for binding sites
285 within tau's MTBR and is thought to promote CHIP-mediated tau degradation and clearance[21,25,62–
286 67]. It is plausible that aggregated tau may form as a consequence of an imbalance in the ratio of
287 Hsp70 vs. Hsp90 binding, which, if shifted towards Hsp70, could radically shift tau processing
288 away from degradation towards stabilization of aggregated tau intermediates. In this scenario,
289 Hsp70 depletion or inhibition would facilitate proteasome or autophagic targeting (degradation)
290 by shifting the balance away from tau refolding. Future proteomics studies will be needed to
291 determine whether distinct tau triage complexes emerge temporally in response to tau aggregation.
292 For example, identifying the PL-SF interactome over time may reveal distinct triage stages in
293 which Hsp70 has shifted from pro-folding to pro-aggregation[19].

294 We did not observe any effect of Hsc70 on tau aggregation. Though highly homologous,
295 Hsc70 is constitutively expressed at ~30-fold higher levels in the brain compared to the inducible
296 Hsp70 isoform[16]. Hsp70, but not Hsc70, overexpression increased the number of MC1-positive
297 neurons by nearly 3-fold (**Figure 3E, F**). Since Hsp70 is more sensitive to redox signaling (via
298 cysteine residue reactivity), its activity towards tau may be more tunable under stress conditions[68].

299 Prior work has shown that the functional outcome of Hsp70-tau interactions is highly
300 dependent on the specificity and fine-tuning provided by co-chaperones that regulate Hsc70[34],
301 Hsp90[69–71] , CHIP[16] , as well as small heat shock proteins[72–74]. Thus, we suspect that many
302 variables could dictate how effectively and efficiently Hsp70 targets tau, including: 1) the extent
303 of MT-dissociated aggregated tau present, 2) the relative balance and abundance of chaperones,
304 co-chaperones, and cofactors that target and triage tau, and 3) the notion that disease onset and

305 disease progression (either acute or chronic) may involve distinct signaling pathways or
306 compensatory responses.

307 Taken together, our study supports the notion that depletion or activity-modifying
308 approaches targeting Hsp70 (or its cofactors and co-chaperones) may be neuroprotective in the
309 context of the AD brain. While brain-specific HSP70 knockout mice are not available (to the best
310 of our knowledge), brain-permeable Hsp70 inhibitors may have therapeutic utility, although broad
311 Hsp70 inhibition could have detrimental effects on overall brain proteostasis. Therapeutic
312 strategies aimed at "precision proteostasis" could selectively modulate chaperone–client
313 interactions to favor the clearance of pathogenic tau without compromising global protein
314 homeostasis and without directly targeting tau itself.

315

316 **Materials and Methods**

317

318 **Plasmid and lentivirus cloning**

319 To generate the pUltra-T40 WT, PL, PL-SF, SF, PL/SF-2Δ (277-278), PL/SF-2Δ (308-309),
320 PL/SF-4Δ, HSC70-flag, HSP70-flag, and HSP90-flag constructs, the cDNAs were amplified
321 through PCR and inserted into the pUltra vector using AgeI and SalI restriction endonucleases to
322 replace eGFP in pUltra. pUltra-XeGFP was made by removing eGFP using AgeI and BspEI,
323 creating a blunt end with Klenow before circularizing. pUltra-T40 WT (eGFP), PL/SF (eGFP),
324 and PL/SF-4Δ (eGFP) were created by replacing TDP43 in pUltra TDP43 WT (eGFP) using BspEI
325 and SalI. To generate PL/SF/2IP, two consecutive Q5 site-directed mutagenesis were performed
326 on PL/SF(eGFP). pUltra was ordered from Addgene (Plasmid #24129). pUltra was a gift from
327 Malcolm Moore (Addgene plasmid # 24129; RRID:Addgene_24129). shRNA plasmids against

328 HSP70 (TRCN0000098597, TRCN0000098598) and HSP90 (TRCN0000008491,
329 TRCN0000008494) were ordered from the UNC Lenti-shRNA Core Facility. Primers used for
330 vector construction are in Table 1.
331
332 **QBI-293 cell culture**
333 QBI-293 (HEK293A) cells (ThermoFisher, #R70507) are commercially available and maintained
334 according to standard protocols. QBI-293 cells were cultured in complete DMEM media (10%
335 fetal bovine serum, 1X L-glutamine, and 1X penicillin/streptomycin). QBI-293 cells were
336 transfected with FuGENE 6 transfection reagent (Promega) to express 2N4R tau constructs for 48
337 hr. Following transfection, cells were lysed and collected in 1X RIPA buffer [50 mM Tris pH 8.0,
338 150 mM NaCl, 5 mM EDTA, 0.5% sodium deoxycholate, 1% Igepal CA-630, 0.1% SDS]
339 supplemented with deacetylase, phosphatase and protease inhibitors: 1 mM phenylmethylsulfonyl
340 fluoride (PMSF), 10 mM Nicotinamide (NCA), 1 mM sodium orthovanadate (Na3VO4), 1 mM
341 sodium fluoride (NaF), 0.5 M β-glycerophosphate, 2 μM Trichostatin A (TSA), and protease
342 inhibitor cocktail composed of L-1-tosylamide-2-phenylethylchloromethyl, N-tosyl-L-lysine
343 chloromethyl ketone, leupeptin, pepstatin, and soybean trypsin inhibitor, each at 1 μg/ml.
344
345 **Primary cortical neuron cell culture**
346 Mouse primary cortical culture was performed in accordance with the University of North Carolina
347 (UNC) Institutional Animal Care and Use Committee (UNC IACUC protocol 24-190). Mouse
348 cortical neurons were dissected and isolated from C57Bl/6 mice (Charles River) at embryonic day
349 15-16 following lethal isoflurane anesthesia. Following anesthesia, embryos were removed from
350 the pregnant abdominal cavity, washed well with ice-cold 70% ethanol and placed in cold Hanks-

351 buffered balanced salt solution (HBSS). Once rinsed, these embryos were moved to a 10cm dish
352 for dissection. The embryos were then removed from the placental membrane and brains were
353 isolated. The cortex was dissected then moved to Hibernate-E solution (BrainBits) with B27
354 (Gibco) and Glutamax (ThermoFisher). The cerebral cortices were minced thoroughly with
355 forceps and incubated for 30 minutes at 37 °C in HBSS with 20 U/mL papain (Worthington
356 Biomedical), 1mM EDTA, 0.2 mg/mL L-Cysteine, and 5U/mL DNAse (Promega). Cortical tissue
357 was further dissociated in plating media (BrainPhys media (Stemcell), 5% fetal bovine serum, 1X
358 B27 (Gibco), 1X penicillin/streptomycin (Gibco), and 1X Glutamax by triturating the sample using
359 a P1000 micropipette. This suspension was centrifuged for 5 minutes at 1.5 rcf to pellet the cells.
360 The pellet was then resuspended in plating media and passed through a 40 µm cell strainer. A
361 Countess 3 automated cell counter (Invitrogen) was used to count the cells. Cells were plated in
362 plating media at 600,000 cells/well in 6-well plates or 30,000 cells/well in 96-well plates. The next
363 day (DIV1), plating media was completely aspirated and replaced with fresh neuronal media
364 (BrainPhys media (Stemcell), B27 (Gibco), 1X penicillin/streptomycin (Gibco), and 1X
365 Glutamax).
366
367 **Lentiviral production**
368 Lentiviral production was performed by co-transfecting 37.5 mg lentivirus plasmid with 25 mg
369 psPAX2, 12.5 mg VSVG, and 6.25 mg REV plasmids per 15 cm culture plates of Lenti-X 293 T
370 cells (Takara). For each lentiviral construct, three 15 cm plates were used for production. Roughly
371 48 hrs after the transfection, cell culture media was collected and subsequently centrifuged at
372 2000 rcf for 10 minutes. Lentiviral particles were purified using a double-sucrose gradient method
373 as follows: supernatants were loaded onto a 70–60% to 30–20% sucrose gradient and centrifuged

374 at 70,000 rcf for 2 hr at 17 °C. The 30–60% fraction containing the viral particles was retrieved,
375 resuspended in PBS, filtered with a 0.45 mm filter flask, loaded onto a 20% sucrose solution, and
376 centrifuged a second time at 70,000 rcf for 2 hr at 17 °C. The supernatants were carefully
377 discarded, and the viral particles in the pellet were resuspended in PBS, aliquoted and stored at
378 − 80 °C.
379

380 **Lentiviral transductions**

381 Primary neurons were transduced with ~3.0×10^{12} viral particles per mL at DIV4 for most
382 experiments (viruses were added at DIV18 for MEA experiments). If neurons were co-transduced
383 with two viruses, both were added sequentially (each at ~3.0×10^{12} viral particles per mL). For
384 transductions, viruses were added directly to the media in each well (1 µl virus per 2 mL media),
385 followed by gentle rocking by hand to distribute viral particles. The following day, virus-
386 containing media was completely aspirated and replaced with half conditioned media (neuronal
387 media from the same neuron culture) and half fresh neuronal media (BrainPhys (StemCell) with
388 B27 (Gibco), Pen-strep (Gibco), and Glutamax (Gibco)). Every two-three days, half of the
389 neuronal media was discarded and replenished with fresh neuronal media until neurons were
390 collected. Most neurons were collected at DIV10 (7 days after transduction), unless otherwise
391 noted.
392

393 **Immunoblotting and biochemical analysis**

394 RIPA soluble lysates (250 µl per well of a 6-well plate) collected from QBI-293 and primary
395 cortical neuron were sonicated 20 times on ice, then centrifuged at 15,000 rcf for 20 minutes at
396 4 °C. The supernatant was removed from the pelleted material, leaving behind a RIPA insoluble

397 pellet. The RIPA insoluble pellet was washed with 250 µl of RIPA lysis buffer with protease,
398 phosphatase, and deacetylase inhibitors and centrifuged at 15,000 rcf for 20 minutes at 4 °C. This
399 supernatant was removed and discarded and 75 µl of 1% SDS was added to each pellet then
400 sonicated 20 times at room temperature. These samples were then centrifuged at 15,000 rcf at room
401 temperature. The supernatant from these tubes was removed and stored in separate tubes as the
402 SDS-soluble fraction. The RIPA and SDS-soluble supernatants were then mixed with 6X loading
403 dye with DTT and boiled at 98 °C for 10 minutes in a PCR thermocycler (BioRad). Samples were
404 run and resolved via SDS-PAGE on 4–20% gradient gels (BioRad). Gels were transferred to iBlot
405 2 Midi nitrocellulose membranes using the iBlot 2 (Invitrogen) following the standard P0, 7-
406 minute settings. Following transfer, membranes were blocked with 2% milk in 1X TBS for 30
407 minutes and then incubated with primary antibody overnight at 4 °C on a rocker. The next day,
408 membranes were incubated with HRP-conjugated anti-mouse or anti-rabbit antibodies (1:1000)
409 for 1-2 hr at room temperature. Blots were developed with ECL Western Blotting substrate
410 (Cytiva, Amsterdam) and imaged on a GE ImageQuant LAS4000.
411

412 **Immunocytochemistry**

413 Immunocytochemistry experiments were performed using QBI-293 cells or cortical primary
414 neurons plated on poly-D-lysine (PDL)-coated 96-well plates. Following either plasmid
415 transfection (48 hr) or lentiviral transduction (7 days unless otherwise stated), cells were washed
416 once in PBS, immediately fixed in 4% paraformaldehyde for 15 minutes, then washed once more
417 with PBS. Following fixation, cells were then permeabilized with permeabilization buffer (0.2%
418 Triton X-100 (Sigma) in PBS) for 20 minutes then blocking buffer (4% normal goat serum in PBS
419 with 0.05% Tween 20) for 1 hr. Primary antibodies were added in blocking buffer and incubated

420 overnight on a rocker at 4 °C. The following day, cells were washed 3X in PBS with 0.05% tween
421 20 and incubated with Alexa 488, Alexa 594, or Alexa 647 conjugated secondary antibodies at
422 1:1000 and DAPI for 1 hr. Cells were then washed 3X in PBS with 0.05% Tween 20. Cells were
423 then imaged using an EVOS M7000 automated microscope with EVOS 20X objective (Invitrogen
424 AMEP4982) and 40X objectives (Invitrogen AMEP4754) and DAPI, GFP, Texas Red, and Cy5
425 light cubes. Note: Some representative images were artificially brightened or contrasted in
426 Microsoft PowerPoint or Celleste 5.0 and 6.0 software (Invitrogen) to aid visualization. Any panels
427 assessing the same set of conditions were brightened to identical levels. Images were not
428 manipulated prior to quantification.
429
430 **Antibodies**
431 The following primary antibodies were used in this study: AT8 (ThermoFisher Scientific-
432 MN1020), AT100 (ThermoFisher Scientific MN1060), AT180 (ThermoFisher Scientific
433 MN1040), TauC3 (ThermoFisher Scientific-AHB0061), T49 mouse tau (Millipore- MABN827),
434 Tau12 (Millipore, MAB2241, 1:1000), Tau5 (AHB0042), Hsp70 used for immunoblotting (Enzo-
435 ADI-SPA-810-D), Hsp70 used for immunoblotting and immunocytochemistry (Cell Signaling
436 Technologies- 4872), Hsc70 1B5 (ADI-SPA-815-F), Hsp90 16F1 (Enzo- adi-spa-835), Total tau
437 rabbit polyclonal- formerly K9JA (DAKO, A0024 1:2000), GAPDH 6C5 (Millipore- MAB374),
438 ac-tubulin (Sigma T7451), alpha tubulin (Sigma, T9026), Anti-FLAG M2 (Sigma, F1804, 1:2000),
439 GFAP (Dako, 20334). The MC1 antibody was kindly shared by Dr. Peter Davies. Quantification
440 of immunoblotting was measured by ImageStudio Lite Version 5.2.
441
442 **Co-immunoprecipitation reactions**

443 All co-immunoprecipitations were performed in QBI-293 cells transfected with plasmids
444 expressing 2N4R wild-type, P301L, P301L/S320F, and P301L/S320F 4Δ for 48 hrs prior to
445 collection. Each well of a 6-well plate was used as separate conditions. Cells were collected in 250
446 µl RIPA buffer with protease, phosphatase, and deacetylase inhibitors prior to co-
447 immunoprecipitation. Lysates were immediately rotated on a wheel for 30 minutes at 20 rpm at 4
448 ºC. Lysates were then centrifuged at 15,000 rcf for 15 minutes at 4 ºC. Supernatants were removed
449 and 40 µl were kept as input. The remaining supernatant was pre-cleared with 50 µl of Protein
450 A/G PLUS-Agarose beads (Santa Cruz, sc2003) for 30 minutes at 4 ºC. Lysates were centrifuged
451 for 1 minute at 1,500 rcf, and the supernatant was removed. The volume of each reaction was
452 brought to 500 µl of RIPA buffer with inhibitors. For each reaction, 8 µl of tau5 antibody was
453 added to each reaction, then 75 µl of agarose protein A/G beads. Lysates were rotated on a wheel
454 at 20 rpm at 4 ºC overnight. The following day, lysates were centrifuged at 1,500 rcf for 5 minutes.
455 Most of the supernatant was carefully removed, followed by washing with 500 µl of RIPA buffer
456 with inhibitors, and lysates were centrifuged at 1,500 rcf for 5 minutes. This wash was repeated
457 four times. After the final wash, loading dye with DTT was directly added to the beads and heated
458 for 10 minutes at 98 ºC with intermittent mixing. These were centrifuged for 30 seconds at 1,500
459 rcf prior to storage at -80 ºC.
460

461 **Purification of recombinant tau**

462 Tau purification methods were adapted from Barghorn et al, 2004[75]. Untagged wild-type and
463 mutant versions of tau were cloned into pRK172 backbone and transformed into BL21(DE3)-RIL
464 cells. Cells were grown in LB media at 37 °C until the OD600 reached 0.8. Protein expression was
465 then induced with IPTG and continued shaking at 37 °C for 3-5 hrs. After the cells were harvested

466 and resuspended in lysis buffer (20 mM MES pH 6.8, 1 mM EDTA, 5 mM DTT, protease
467 inhibitors benzamidine and leupeptin, and PMSF), the cells were lysed via sonication. Lysed cells
468 were heat shocked at 80 °C for 20 minutes, then centrifuged at 17,500 rpm (36,635 xg) for 30
469 minutes to remove cell debris. Clarified lysate was dialyzed overnight at 4 °C into wash buffer (20
470 mM MES pH 6.8, 50 mM NaCl, 1 mM EDTA, 1 mM $MgCl_2$, 2 mM DTT). Following overnight
471 dialysis, lysates were centrifuged at 17,500 rpm (36,635 xg) for 30 minutes to remove precipitated
472 proteins and then subjected to cation exchange chromatography. The protein was eluted by
473 increasing salt concentration in buffer to 250 mM. The samples were further purified via size
474 exclusion chromatography on a Superdex 200 Increase 10/300 GL column in sizing buffer (25 mM
475 HEPES pH 7.5, 100 mM NaCl, 5 mM $MgCl_2$, 1 mM DTT). Samples were then concentrated as
476 needed using centrifugal filters and flash frozen for later use.
477

478 **Heparin-induced tau aggregation assays:**

479 Tau aggregation assays were carried out in a PolarStar Omega microplate reader using Thioflavin
480 T (ThT) fluorescence to monitor formation of tau aggregates. Aggregation reactions were started
481 by combining 5 μM tau, 2 μM heparin, and 20 μM ThT in reaction buffer (1x PBS, 2 mM TCEP)
482 and transferred to a costar 96-well half-area microplate (black polystyrene, flat bottom, non-
483 treated). The microplate was covered with an ELISA plate sealer and placed in the microplate
484 reader at 37 °C. Fluorescence measurements were taken every 5 minutes for 12 hrs using a 440-
485 10 nm excitation and 485-12 nm emission filter.
486

487 **HSP70 and HSP90 shRNA knockdown**

488 All shRNAs were obtained from UNC Lenti-shRNA core facility and cloned into the pUltra

489 vectors. Sequences: HSP70 shRNA: GCAGGTGAACTACAAGGGCGA; eGFP control shRNA:
490 TACAACAGCCACAACGTCTAT (Y145 to Y151 residues of eGFP). HSP70 shRNAs were
491 added to the neuron culture four days after transduction with tau lentiviruses at a titer of ~3.0×10^{12}
492 viral particles per mL. Media was half exchanged for fresh neuronal media every two days. After
493 an additional four days in culture, primary neurons lysates were collected for experiments. We
494 noted some toxicity after more than 4 days in culture with HSP70 shRNAs. HSP90 shRNAs were
495 applied for 7 days in culture (~3.0×10^{12} viral particles per mL) prior to collection for experiments
496 and were not overtly toxic.

497 **Multi-electrode array recordings and analysis**

498 Following dissection, primary mouse cortical neurons were directly plated onto poly-D lysine
499 coated 24-well BioCircuit MEA plates (Axion Biosystems). A 10 µl droplet of neurons at a
500 concentration of 16,000,0000 neurons/mL was added directly to the center of each well. Neurons
501 were incubated at 37 °C for 1 hr then 250 µl of plating media (BrainPhys media (Stemcell), 5%
502 fetal bovine serum, 1X B27 (Gibco), 1X penicillin/streptomycin (Gibco), and 1X Glutamax) was
503 carefully added to each well in a circular motion. Following another 1-hr incubation, another 250
504 µl of plating media was added to each well (total volume = 500 µl). The following day, ~90% of
505 plating media was aspirated and fresh neuronal (BrainPhys media (Stemcell), B27 (Gibco), 1X
506 penicillin/streptomycin (Gibco), and 1X Glutamax) media was added to each well. Half of the
507 media was exchanged for fresh neuronal media every two days. At DIV18, neurons underwent an
508 initial, 10-minute pre-recording using the Axion Maestro Edge (Axion Biosystems) and AxIS
509 Navigator software (Axion Biosystems). Immediately following this recording, neurons were
510 transduced with lentiviruses at ~3.0×10^{12} viral particles per mL (four replicate wells per condition).
511 The following day, neuronal activity was recorded for 10 minutes, then lentivirus-containing

512 neuronal media was completely replaced with half fresh neuronal media and half conditioned
513 neuronal media from the same culture. Neurons were recorded nearly every day for 10 minutes
514 and half of the neuronal media was replaced every 2-3 days after recording until DIV71 (day 53
515 of recording). Post-hoc analysis was performed using the NeuralMetricTool (Axion Biosystems)
516 using default analysis options. Data was exported into Microsoft Excel, then graphed via GraphPad
517 Prism 10 for statistical analyses and graphing. Raster plots were generated from the same data
518 using the AxIS Metric Plotting Tool. 96 well plates were plated at the same time using the same
519 primary neurons, underwent identical media changes, and were used for immunocytochemistry at
520 DIV29 and DIV62 in Figure 5.
521

522 **Post-synaptic density isolation**

523 Primary mouse cortical neurons from wild-type C57/BL6 mice were plated on poly-D-lysine
524 coated 6-well plates at 600,000 cells/well. Neurons were treated with lentivirus at DIV4 (1 6-well
525 plate per condition) and half-fed every two days until DIV14. At DIV14, neurons were rinsed in
526 cold PBS and all 6-wells of each plate were collected in a total of 900 µl of homogenization buffer
527 (320 mM sucrose, 5 mM sodium pyrophosphate, 1 mM EDTA, 10 mM HEPES pH 7.4) with
528 protease/phosphatase inhibitor cocktail 200 nM okadaic acid, 1 mM orthovanadate, 1X protease
529 inhibitor cocktail (Roche). Neuronal lysates were homogenized by passing the lysate 12 times
530 using a 26g needle. For each condition, 70 µl of lysate was kept and stored as whole cell lysate.
531 The remaining lysate was centrifuged at 1,000 g for 10 minutes at 4 °C *to* generate pelleted nuclear
532 fraction (P1) and supernatant fraction (S1). The S1 fraction was centrifuged at 15,000 g for 20
533 minutes at 4 °C to generate the membrane/crude synaptosome pelleted fraction (P2) and cytosolic
534 supernatant fraction (S2). The P2 fraction was resuspended in 500 µl of ultrapure H_20 with

535 protease/phosphatase cocktail. 20 µl of 100 mM HEPES was added to the 500 µl of suspension to
536 yield 4 mM HEPES pH 7.4. These samples were then spun on a wheel for 30 minutes at 4°C then
537 centrifuged for 20 minutes at 4 °C at 25,000 g using a Sorvall mTX 150 ultracentrifuge (Thermo
538 Scientific) to generate pelleted synaptic fraction (LP1) and supernatant fraction (LS2). The LP1
539 pellet was resuspended in 250 µl mM HEPES pH7.4 using repeated trituration with a micropipette.
540 This was then mixed with 250 µl of 1% Triton X-100 with protease/phosphatase cocktail and spun
541 on a wheel for 10 minutes at 4 °C. This was then centrifuged in Sorvall mTX 150 ultracentrifuge
542 (Thermo Scientific) at 32,000 g for 20 minutes at 4 °C. This pellet was resuspended in 80 µL of
543 50 mM HEPES pH7.4 using micropipette trituration to yield the PSD fraction. Only total
544 homogenate and PSD fraction were processed and analyzed by SDS-PAGE.
545
546 **Imaging quantification**
547 All immunocytochemistry (aside from organotypic slice cultures) quantification was performed
548 using Celleste 5.0 and 6.0 software (Invitrogen). The number of inclusions were counted using the
549 count/size function. Puncta and inclusions were manually segmented based on intensity (Segment:
550 Manual) and size (Region: Area) thresholds for each tau probe (e.g. AT8, MC1, ThioS). These
551 threshold settings were then applied to all images used for that specific experiment, automatically
552 batched processed using a segment-count-export macro generated in Celleste, then exported to
553 Microsoft Excel for subsequent analysis.
554
555
556 **Hippocampal slice cultures**
557 Sprague-Dawley rats (Charles River Laboratories, Wilmington, MA) were housed and maintained
558 in accordance with the recommendations from the Guide for the Care and Use of Laboratory

559 Animals from the National Institutes of Health, and in accordance with an approved protocol from
560 the Institutional Animal Care and Use Committee of the University of North Carolina-Pembroke.
561 Brain tissue from postnatal 12-day-old rats was rapidly prepared and hippocampi positioned on a
562 McIlwain tissue chopper for assembling slices for interface cultures as previously described[76,77].
563 Three-dimensional organotypic cultures of specific brain regions are well known for studying
564 different types of physiologies and pathogenic processes[78–80]. Transverse hippocampal slices (400-
565 μm thickness) were immediately placed in ice-cooled-buffer solution (pH 7.2) then transferred in
566 groups of eight to nine onto the Biopore membrane of culture inserts (Millipore, Billerica, MA).
567 The media below the culture inserts contained 50% basal medium eagle (Sigma-Aldrich, St. Louis,
568 MO), 25% Earle's balanced salts (Sigma-Aldrich), 25% horse serum (Gemini Bio-Products,
569 Sacramento, CA), and defined supplements as previously described[81] . The media were initially
570 changed 24 hrs after the slicing procedure, followed by subsequent changes every 3-4 days. The
571 cultivated hippocampal slices were maintained under conditions of a 5% CO2-enriched
572 atmosphere at a constant temperature of 37 °C for a duration of nine weeks.

573 **Lentiviral infection of organotypic cultures**

574 Lentiviruses expressing GFP or GFP-tagged tau variants (wild-type, PL-SF, and PL-SF 4Δ tau).
575 For each condition, 1.5 μl of lentivirus were applied onto the surface of individual organotypic
576 slices (~7.5×10^{12} viral particles per slice) approximately 3 hrs after the placement of the slices on
577 Millipore inserts. Following a nine-week incubation period in vitro, both the infected organotypic
578 slices and their corresponding controls were fixed with 4% PFA for 3-4 hrs. Subsequently, the
579 slices were rinsed multiple times with PBS and stored in PBS at 4 ºC.

580

581 **Immunofluorescence staining and imaging of organotypic brain slice cultures**

582 The fixed organotypic hippocampal explants underwent permeabilization in PBS containing 0.5%
583 Triton-X100 for 30 minutes. Following this, the slices were blocked with a solution of 5% BSA in
584 PBS containing 0.1% Triton-X100 for 90 minutes at room temperature. Subsequently, the
585 organotypic slices were incubated for 48 hrs at 4 ºC with primary antibodies targeting AT8 (1/400;
586 ThermoFisher Scientific- MN1020) or MC1 (1/400; Dr. Peter Davies, diluted in a solution of 3%
587 BSA containing 0.1% Triton-X100. Next, brain explants were washed 3-4 times with PBS
588 containing 0.1% Triton-X100 and then exposed to Goat anti-mouse IgG Alexa-FluorTM 568
589 (ThermoFisher, Waltham, MA) for 120 minutes at room temperature. Following this incubation,
590 the organotypic slices were rinsed three times with PBS containing 0.1% Triton-X100. During the
591 second wash, NucBlue stain (Invitrogen, MA, USA) was introduced to the PBS to promote DAPI
592 nuclear staining. Subsequently, the slices were rinsed in PBS and were mounted onto glass slides,
593 covered by 1.5 mm coverslips, using ProlongTM diamond antifade mountant (Thermo Fisher
594 Scientific, NC, USA). Immunofluorescence images were captured with Andor Dragonfly spinning
595 disk confocal using the Zyla Plus 4.2MP sCMOS (Oxford Instruments, Abingdon, United
596 Kingdom). Image our blinded processed adopting the equal adjust using the Imaris
597 Multidimensional visualization and analysis software (Schlieren-Zurich, Switzerland).
598

599 **Human brain fractionation**

600 Human control and Alzheimer's disease (AD) cortical brain tissues (Braak stages V–VI) were
601 obtained from the Center for Neurodegenerative Disease Research brain bank at the University of
602 Pennsylvania. Gray matter from the frontal cortex of each subject was isolated and homogenized
603 in 3 volumes per gram (vol/g) of cold high-salt RAB buffer (0.75 M NaCl, 100 mM Tris, 1 mM
604 EGTA, 0.5 mM $MgSO_4$, 0.02 M NaF, 2 mM DTT, pH 7.4), supplemented with deacetylase,

605 phosphatase, and protease inhibitors as previously described. Homogenates were incubated at 4 °C
606 for 20 minutes to facilitate microtubule depolymerization, followed by ultracentrifugation at
607 100,000 × g for 30 minutes at 4 °C. The resulting supernatant was designated the high-salt fraction.
608 The pellet was then re-homogenized and subjected to a second round of centrifugation under
609 identical buffer and conditions. After removal of the supernatant, the remaining pellets were
610 homogenized in 5 vol/g of cold RIPA buffer (50 mM Tris, pH 8.0, 150 mM NaCl, 1% NP-40, 5
611 mM EDTA, 0.5% sodium deoxycholate, 0.1% SDS), and centrifuged once more at 100,000 × g
612 for 30 minutes at 4 °C. Subsequent to myelin flotation, the pellets were re-extracted in RIPA buffer
613 containing 20% sucrose to eliminate residual myelin and labeled as the RIPA fraction. Finally, the
614 insoluble material was extracted using 1 vol/g of urea extraction buffer (7 M urea, 2 M thiourea,
615 4% CHAPS, 30 mM Tris, pH 8.5). Both the high-salt and urea-soluble fractions were subjected to
616 SDS-PAGE followed by immunoblotting with antibodies targeting Hsp70, Hsc70, and GAPDH.
617

618 **Human brain immunohistochemistry and confocal microscopy**

619 Human hippocampal tissue sections mounted on coverslips were obtained from the UNC
620 Translational Pathology Laboratory (TPL), which oversees a cataloged and archived repository of
621 Alzheimer's disease (AD) brain specimens, including neuropathologically confirmed cases from
622 UNC-affiliated donors. The 10 um sections were de-paraffinized with two 45-minute washes in
623 xylene followed by one-minute washes in 100% ethanol (x2), 95% ethanol, 80% ethanol, 75%
624 ethanol, water, and finally allowed to soak O/N in 1x PBS. Antigen retrieval is performed using a
625 citrate-based antigen unmasking solution (Vector Labs, H-3300-250) in boiling Mill-Q water for
626 10-minutes. The slides were then washed 3x5-min with TBS, followed by 1x wash in TBS + 0.1%
627 TritonX-100 for 20 minutes, 3x5-min with TBS, and 1x5 min in 3% Goat Serum in TBS (Southern

628 Biotech, 0060-01). Sections were then stained 2x O/N in a humidified chamber at room
629 temperature using anti-AT8 (1:500, Invitrogen, MN1020) and anti-Hsp70 (1:500, Abcam,
630 ab181606). Slides were then washed 3x5-min with TBS followed by secondary staining with goat
631 anti-mouse IgG 488 (1:1000, Invitrogen, A-11001) and goat anti-rabbit IgG 594 (1:1000,
632 Invitrogen, A-11012) for 24 hours at 4°C in a dark, humidified chamber. Slides were then washed
633 3x5-min with TBS, allowed to dry, and mounted with Fluoromount-G with DAPI (Invitrogen, 00-
634 4959-52).
635 Confocal microscopy was performed on an LSM980 (Zeiss) inverted laser scanning confocal
636 microscope. The LSM980 is equipped with a motorized X, Y, stage and Z-focus with high-speed
637 Piezo insert along with four diode lasers (405, 488, 561, and 633). Images were acquired with 1x
638 Nyquist sampling using 63x 1.4 NA Plan-Apochromat oil objective (Zeiss) and 4 channel GaAsP
639 detectors on Zen Blue 3.6 software. Images were acquired with 1x Nyquist sampling using 20x
640 0.8 NA Plan-Apochromat air objective (Zeiss) and 4 channel GaAsP detectors on Zen Blue 3.6
641 software.
642
643 **Statistical analysis**
644 GraphPad Prism 10 software was used for all statistical analyses. For comparisons between two
645 groups, two-tailed unpaired Student's t-tests were used. For multiple group comparisons, one-way
646 ANOVA followed by Dunnet's or Sidak's post hoc tests were applied as appropriate. Results were
647 polled from a minimum of n=3 independent experiments and presented as mean ± standard error
648 of the mean (SEM). P-values < 0.05 were considered statistically significant. The number of
649 replicates (n) and details of the specific tests applied are provided in figure legends.
650

652 **Funding Declaration**

653 Support for this work was provided by National Institutes of Health (NIH) grants F32AG072826
654 (MRB) and R01AG068063 (TJC). This study was supported by the National Institute on Aging of
655 the National Institutes of Health under Award Number P30AG072958 (NIAP30AG072958)
656 (MRB, MA, and JHT), Alzheimer's Association grants AARG-22-924321 (TJC) AARF22926617
657 (JHT), and CurePSP grant 656-2018-06 (TJC). The content is solely the responsibility of the
658 authors and does not necessarily represent the official views of the National Institutes of Health.

659

660 **Acknowledgements**

661 The Andor Dragonfly microscope was funded with support from National Institutes of Health grant
662 S10OD030223. The Zeiss LSM 980 microscope was funded with support from NIH grant S10
663 OD032388. We would also like to thank Kinsley Adams for her expertise and assistance with the
664 hippocampal organotypic slice cultures. We would also like to thank the University of
665 Pennsylvania (Center for Neurodegenerative Disease Research brain bank) for providing human
666 control and AD cortex lysates. Lastly, we would like to thank the University of North Carolina
667 Translational Pathology Laboratory for providing AD hippocampal brain sections.

668

669 **Conflict of interest**

670 The authors declare that they have no conflicts of interest with the contents of this article.

671

672 **Author Contributions**

673 MRB designed and performed most experiments. MA, JS, and BB designed and carried out ex
674 vivo organotypic slices experiments and imaging. KP performed all immunohistochemistry and

675 confocal imaging of human post-mortem brain. CO assisted with co-immunoprecipitation
676 experiments and post-synaptic density preparations. CO and JHT performed human brain
677 fractionation and immunoblots. EP performed all protein purification and carried out the
678 Thioflavin T aggregation assays. JMM assisted with multi-electrode array recordings and
679 analyses. XT prepared all plasmid and lentiviral constructs for all experiments. DK and HT
680 designed and performed the QBI293 experiments comparing various P301 and S320 tau mutants.
681 JHT, JS, NB, and BB provided additional experimental guidance and interpretation. MRB and TJC
682 prepared the manuscript and figures. TJC directed and supervised the study. All authors consented
683 and contributed to the final version of the manuscript.
684
685

686 **Figures and Figure Legends**

Bryan et al., Figure 1.

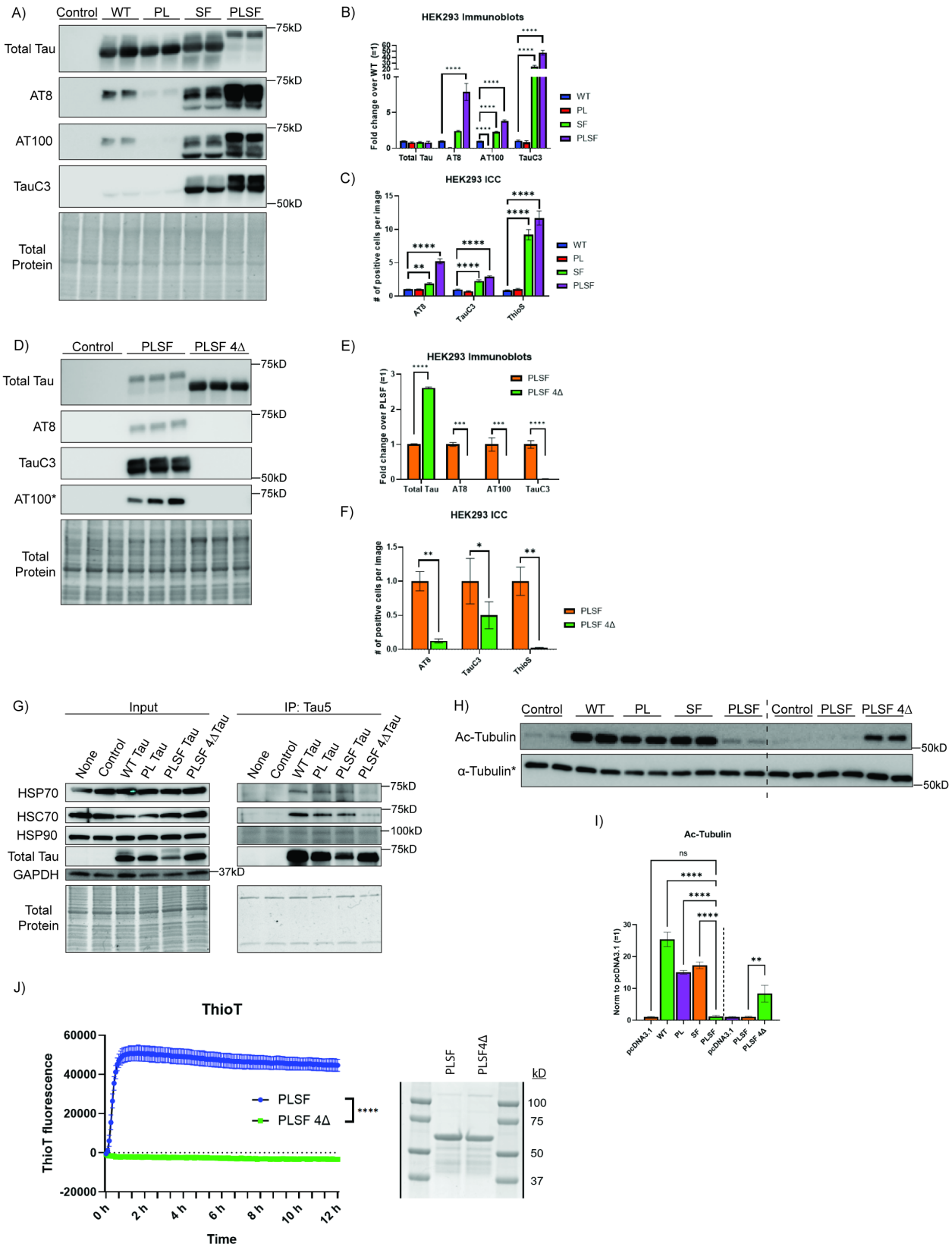

688 **Figure 1: Abrogating tau binding to heat shock proteins alleviates pathology in a PL-SF tau**
689 **aggregation model.**
690 **A)** Representative immunoblots (RIPA fraction) of QBI-293 cells transfected with 2N4R WT,
691 P301L, S320F, or P301L-S320F tau. **B)** Immunoblot quantification of total tau, p-tau (AT8 and
692 AT100), and cleaved tau (TauC3) in RIPA fraction. N=4 per condition; **C)** Immunocytochemistry
693 quantification of QBI-293 cells transduced with WT, P301L, S320F, or PL-SF tau labeled with
694 AT8, TauC3, or ThioS. N=48 FOVs per condition. *= p-value significant by one-way ANOVA.
695 Representative images found in Supplemental Figure 1. **D)** Representative immunoblots (RIPA
696 fraction) of QBI-293 cells transfected with 2N4R P301L-S320F tau or P301L-S320F 4Δ (deletion
697 of I277/278, I308/V309 residues). *AT100 was run on a separate blot with the exact same lysates
698 to improve detection. **E)** Immunoblot quantification of total tau, p-tau (AT8 and AT100), and
699 cleaved tau (TauC3) in RIPA soluble fractions. N=3 per condition. **F)** Immunocytochemistry
700 quantification of QBI-293 cells transduced with 2N4R PL-SF or PL-SF 4Δ tau labeled with AT8,
701 TauC3, or ThioS. N=16 FOVs per condition. *= p-value significant by unpaired Student's t-test.
702 Representative images found in Supplemental Figure 3. **G)** Co-immunoprecipitation of QBI-293
703 cells transfected with WT, P301L, PL-SF, or PL-SF 4Δ tau. Tau5 antibody was used to IP tau and
704 immunoblots were probed with total tau (rabbit polyclonal) and Hsp70, Hsc70, and Hsp90
705 antibodies. **H)** Representative immunoblots of QBI-293 cells transfected with 2N4R tau variants
706 and probed with acetyl-tubulin and total alpha-tubulin antibodies. Note: Acetyl tubulin and alpha
707 tubulin blots were run separately with the same lysates to improve detection. **I)** Quantification of
708 acetyl-tubulin across all 2N4R tau variants. -- line signifies separate sets of transfections in panel
709 I and J. N=4 per condition; *= p-value significant by one-way ANOVA. Control= empty plasmid
710 vector (pcDNA3.1)**.** **J)** Quantification of in vitro Thioflavin T aggregation assay using purified

711 protein from PLSF and PLSF 4Δ. N=4 replicates per condition. *= significant by unpaired student

712 t-test at 12hr timepoint. Coomassie (right) shows equal protein loading into reactions.

713

Bryan et al., Figure 2.

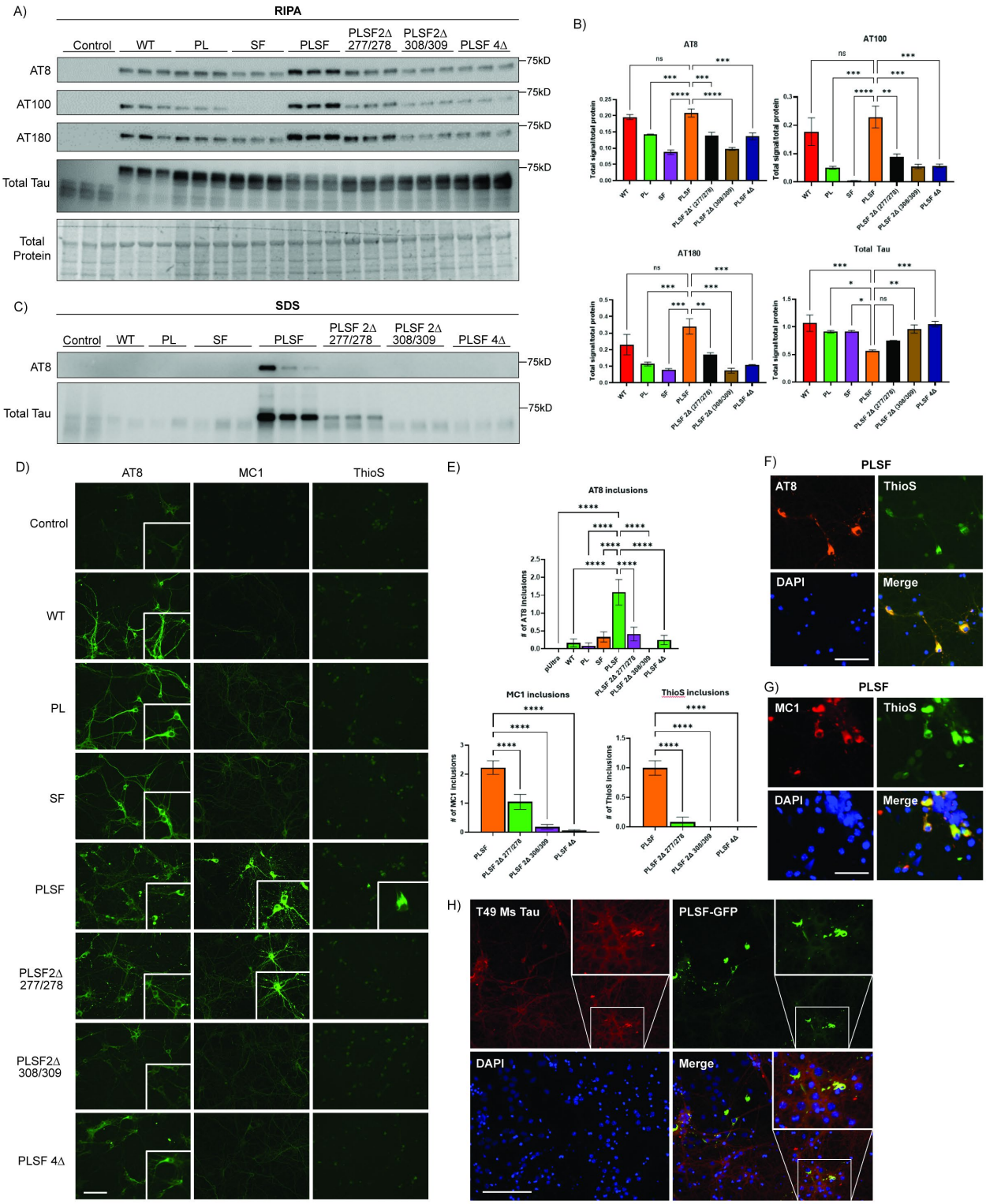

Figure 2: Development and characterization of a PL-SF tau aggregation model in primary cortical neurons.

717 **A)** Representative RIPA-soluble immunoblots of DIV10 primary cortical neurons transduced with
718 lentiviruses expressing 2N4R WT, P301L, S320F, P301L-S320F, or PL-SF 2Δs (R2 and R3) and
719 4Δ tau variants. **B)** Quantification of AT8, AT100, AT180, and total tau immunoblots in primary
720 cortical neurons (RIPA fraction). N=3 per condition; *= p-value significant by one-way ANOVA.
721 **C)** Representative SDS-soluble immunoblots of DIV10 primary cortical neurons transduced with
722 lentiviruses expressing 2N4R WT, P301L, S320F, P301L-S320F, or PL-SF 2Δ and 4Δ tau variants.
723 N=2 for control, WT, and P301L; N=3 for other variants. **D)** Representative immunocytochemistry
724 images of 2N4R tau variants labeled with AT8 (p-tau), MC1 (conformational tau), ThioS
725 (aggregated tau) in GFP. Scale bar= 125 µm. **E)** Quantification of the number of AT8, MC1, and
726 ThioS inclusions in PL-SF and PL-SF 2Δ (R2 and R3) and 4Δ variants. N=12-24 FOVs per
727 condition. *= significant by one-way ANOVA. **F, G)** Representative immunocytochemistry
728 images of PL-SF tau displaying colocalization between F) AT8 (p-tau) or G) MC1 (conformational
729 tau) with ThioS (aggregated tau). Scale bar= 50um. **H)** Representative immunocytochemistry of
730 PL-SF GFP colocalized with T49 tau (mouse-specific). Scale bar= 125 µm. Control= empty viral
731 vector (pUltra)**.**

Bryan et al., Figure 3.

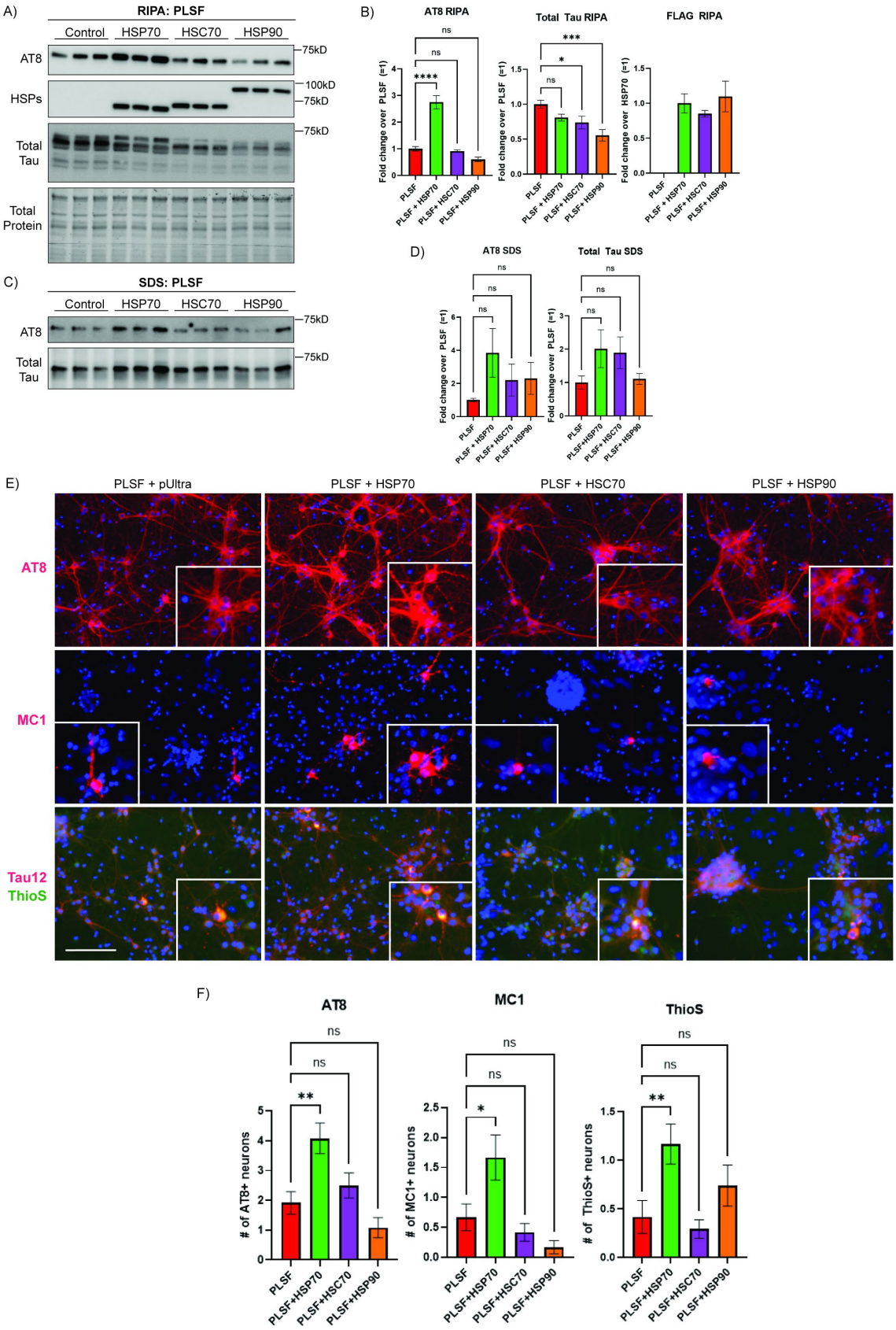

733 **Figure 3: Hsp70 exacerbates tau hyperphosphorylation and aggregation.**

734 **A)** Representative immunoblots of 2N4R PL-SF tau co-transduced with HSP70, HSC70, and
735 HSP90 in DIV10 primary cortical neurons (RIPA fraction). **B)** Quantification of AT8 (p-tau), total
736 tau (rabbit polyclonal), or Hsp70, Hsc70, Hsp90 (FLAG-tagged) in the RIPA fraction. N=6 per
737 condition. *= p-value significant by one-way ANOVA. **C)** Representative immunoblots of 2N4R
738 PL-SF tau co-transduced with HSP70, HSC70, and HSP90 in DIV10 primary cortical neurons
739 (SDS fraction). **D)** Quantification of AT8 (p-tau), total tau (rabbit polyclonal) in the SDS fraction.
740 N=6 per condition. ns= p-value is not significant by one-way ANOVA. **E)** Representative
741 immunocytochemistry images of primary cortical neurons co-transduced 2N4R PL-SF tau and
742 HSP70, HSC70, or HSP90 labeled with AT8, MC1, Tau12 (RFP) or ThioS (GFP). Scale bar= 125
743 μm. **F)** Quantification of MC1, AT8, and ThioS positive inclusions in primary cortical neurons
744 co-transduced 2N4R PL-SF tau and either HSP70, HSC70, or HSP90. n=12 FOVs per condition.
745 *= p-value significant by one-way ANOVA. Control= empty viral vector (pUltra)**.**

746

Bryan et al., Figure 4.

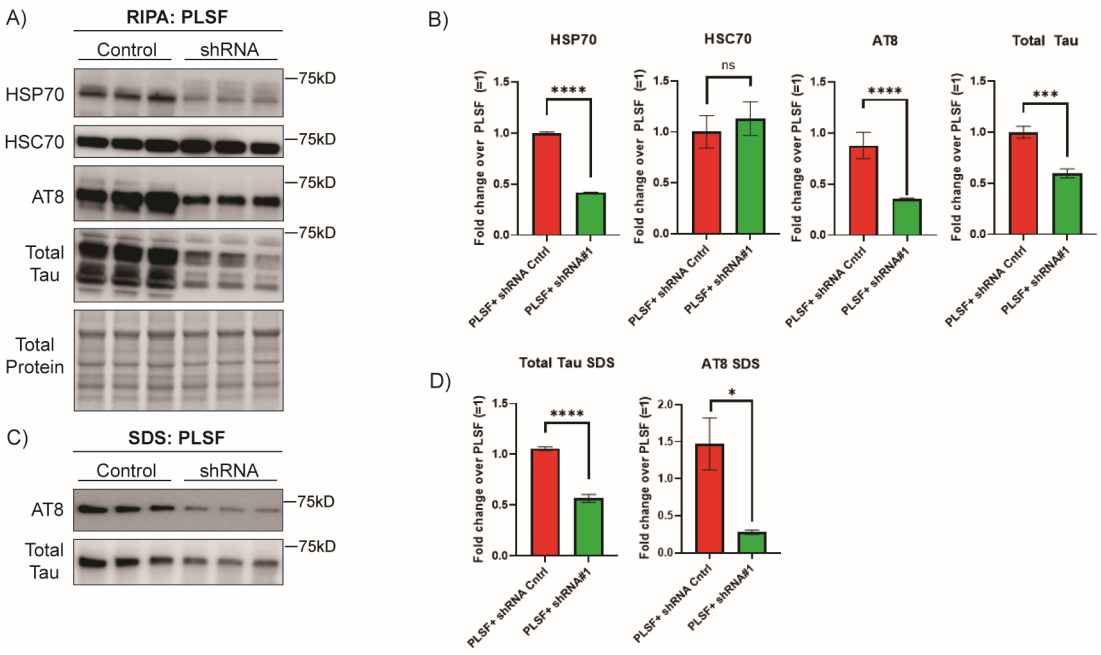

Figure 4: Reducing Hsp70 can suppress tau hyper-phosphorylation and aggregation. **A)** Representative immunoblots of 2N4R PL-SF tau co-transduced with a shRNA against HSP70 in DIV10 primary cortical neurons (RIPA fraction). **B)** Quantification of AT8 (p-tau), total tau (rabbit polyclonal) and endogenous Hsp70 and Hsc70 in the RIPA fraction. N=3. **C)** Representative immunoblots of 2N4R PL-SF tau co-transduced a shRNA against HSP70 in DIV10 primary cortical neurons (SDS fraction). **D)** Quantification of AT8 (p-tau), total tau (rabbit polyclonal) in the SDS fraction. N=3. *= p-value significant by unpaired Student's t-test. Control= empty viral vector (pUltra)**.**

Bryan et al., Figure 5.

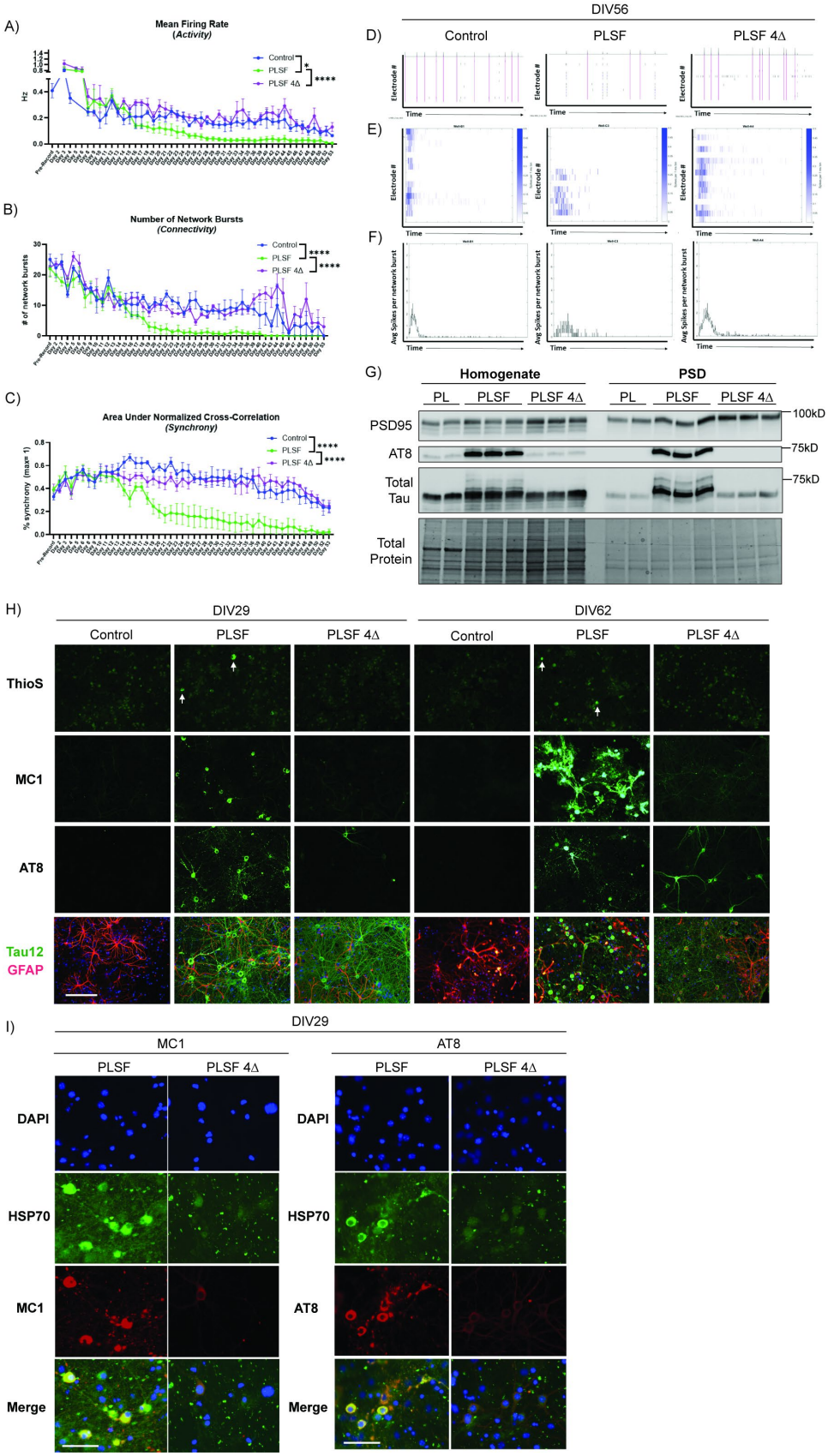

757 **Figure 5: Mature tau aggregates cause functional deficits in neurons that are reversed by**
758 **abrogating tau-Hsp binding.**

759 **A-C)** Quantification of neuronal activity comparing PL-SF to PL-SF 4Δ across 53 days of multi-
760 electrode array recording starting at DIV18 following initial pre-recording. A) Mean firing rate-
761 activity B) Number of network bursts- connectivity C) Area under normalized cross-correlation-
762 synchrony. N=4 replicate wells per condition. *= p-value significant by one-way ANOVA. **D-F)**
763 Representative raster and network burst plots at DIV54 (day 36 of recording) comparing empty
764 control (pUltra) to PL-SF and PL-SF 4Δ. D) Number of network bursts across electrodes over time
765 (pink lines) E) number of spikes across electrodes over time F) Average number of spikes per
766 network burst over time. **G)** Representative immunoblot of isolated post synaptic density (PSD)
767 in DIV18 primary cortical neurons transduced with lentiviruses expressing P301L, PL-SF, or PL-
768 SF 4Δ. Immunoblot was probed with PSD95, AT8 (p-tau), and rabbit polyclonal tau (total tau). **H)**
769 Representative 20X immunocytochemistry images of primary cortical neurons comparing empty
770 vector control (pUltra) to PL-SF and PL-SF 4Δ tau variants at DIV29 and DIV62. Neurons were
771 labeled with ThioS (aggregated tau), MC1 (conformational tau), AT8 (p-tau), and Tau12 (total
772 tau) in GFP. Tau12 was co-labeled with GFAP (RFP) to label astrocytes. Scale bar= 125 µm. **I)**
773 Representative immunocytochemistry images of primary cortical neurons comparing PL-SF and
774 PL-SF 4Δ at DIV29. Neurons were labeled with endogenous Hsp70 (GFP), MC1 or AT8 (RFP),
775 and DAPI (BFP). Scale bar= 50 µm. Control= empty viral vector (pUltra)**.**

Bryan et al., Figure 6.

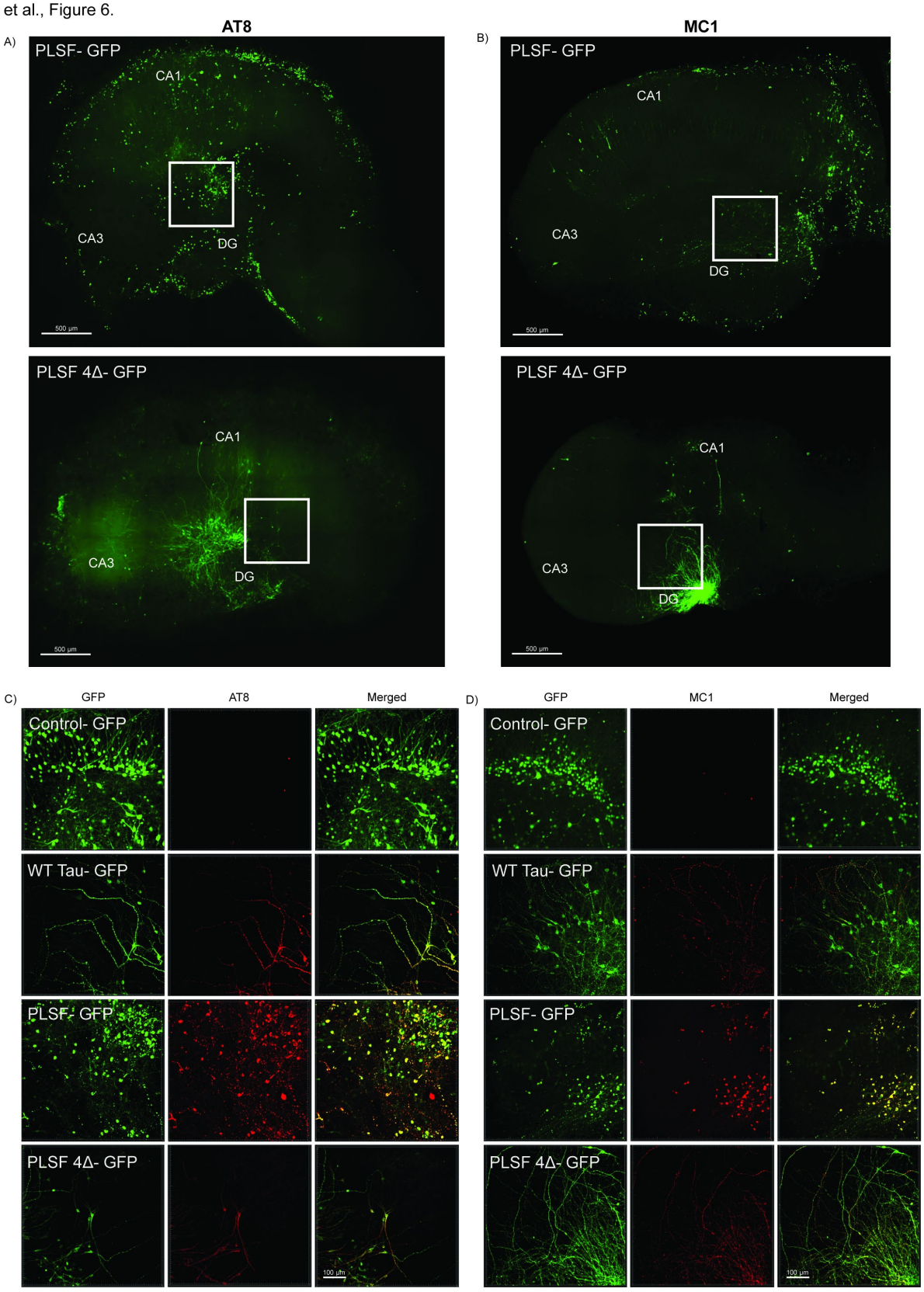

777 **Figure 6: Abrogating tau-Hsp binding suppresses tau pathology in three-dimensional**
778 **organotypic hippocampal slice cultures.**
779 Rat hippocampal slices were processed for immunocytochemistry after 9 weeks in culture
780 following lentiviral infection of eGFP empty vector control, wild-type tau, PL-SF tau, and PL-SF
781 4Δ. **A, B)** Immunocytochemistry of the entire hippocampal slice following labeling of reveal
782 sufficient expression of PL-SF and PL-SF 4Δ lentiviruses (GFP). Left- AT8 staining; Right- MC1
783 staining. CA1, CA3, and DG regions are labeled in white font. White boxes denote magnified
784 images in panel C, D. Scale bar= 500 µm. **C, D)** Representative immunocytochemistry images of
785 C) AT8 and D) MC1 labeled in RFP for empty vector control, wild-type tau, PL-SF tau, and PL-
786 SF 4Δ taken from the dentate gyrus (DG) region of the hippocampal slice culture (inset white
787 boxes from A, B). Scale bar= 100 µm.

Bryan et al., Figure 7

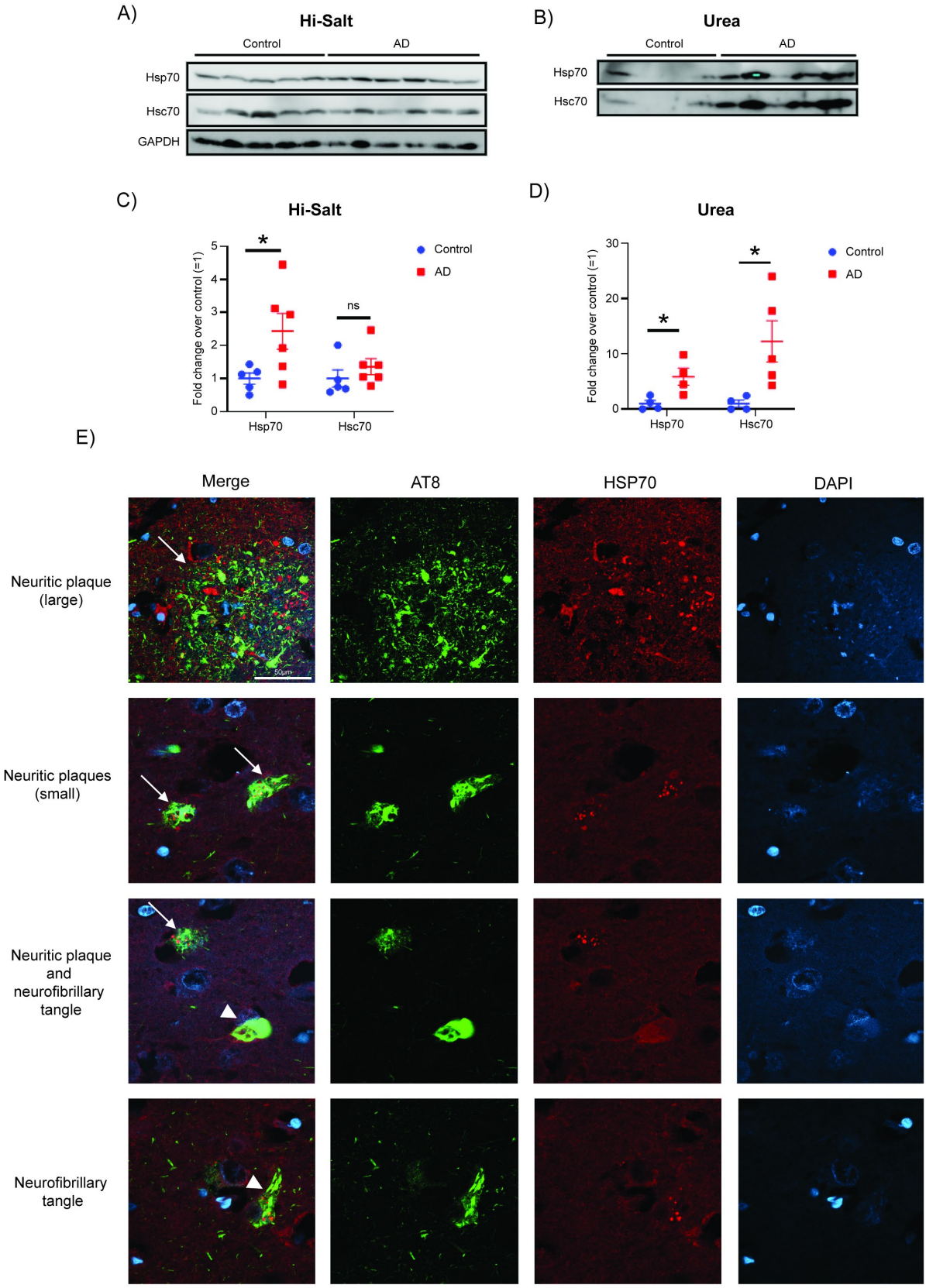

789 **Figure 7: HSP70 is upregulated in human AD brain and intercalates within tau aggregates.**
790 **A)** Hi-Salt soluble immunoblots from control (n=5) and AD (n=6) cortical lysates probed for
791 Hsp70, Hsc70, and GAPDH. **B)** Quantification of hi-salt immunoblots. *= p-value significant by
792 unpaired Student's t-test. **C)** Urea soluble immunoblots from control (n=4) and AD (n=5) probed
793 for Hsp70 and Hsc70. **D)** Quantification of urea immunoblots. *= p-value significant by unpaired
794 Student's t-test. Overexposed Hsp70 AD sample in urea was excluded from quantification. **E)**
795 Representative 63X confocal single-plane z-stacks from AD human hippocampus stained with
796 AT8 (p-tau) and Hsp70. White arrow label neuritic plaques and white arrowheads label NFTs.
797
798
799
800

Bryan et al., Supplemental Figure 1.

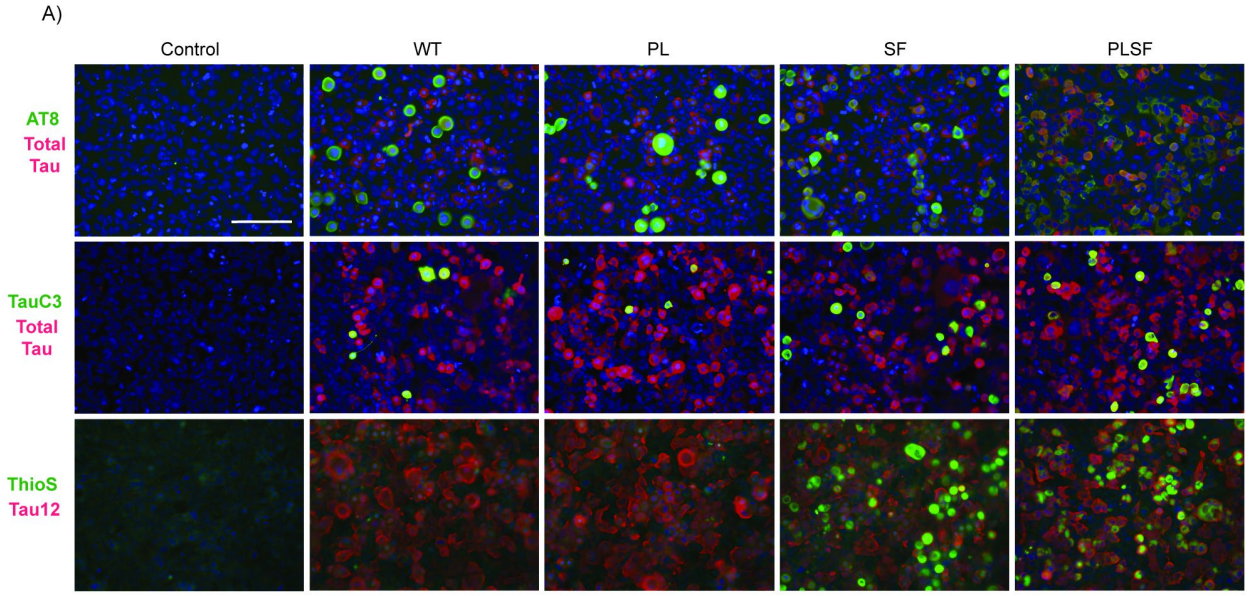

801

802 **Supplemental Figure 1: Accelerated PL-SF aggregation compared to single tau mutants in**

803 **immortalized cell lines.**

804 **A)** Representative immunocytochemistry images from QBI-293 cells expressing empty vector

805 (pcDNA) or WT, PL, SF, and PL-SF tau variants. Cells were labeled with AT8 (p-tau) or TauC3

806 (C-terminal cleaved tau) with rabbit polyclonal tau (total tau) and ThioS with Tau12 (human tau).

807 Quantification of images is found in Figure 1C. Control= empty plasmid vector (pcDNA3.1). Scale

808 bar= 125 µm.

809

810

811

Bryan et al., Supplemental Figure 2.

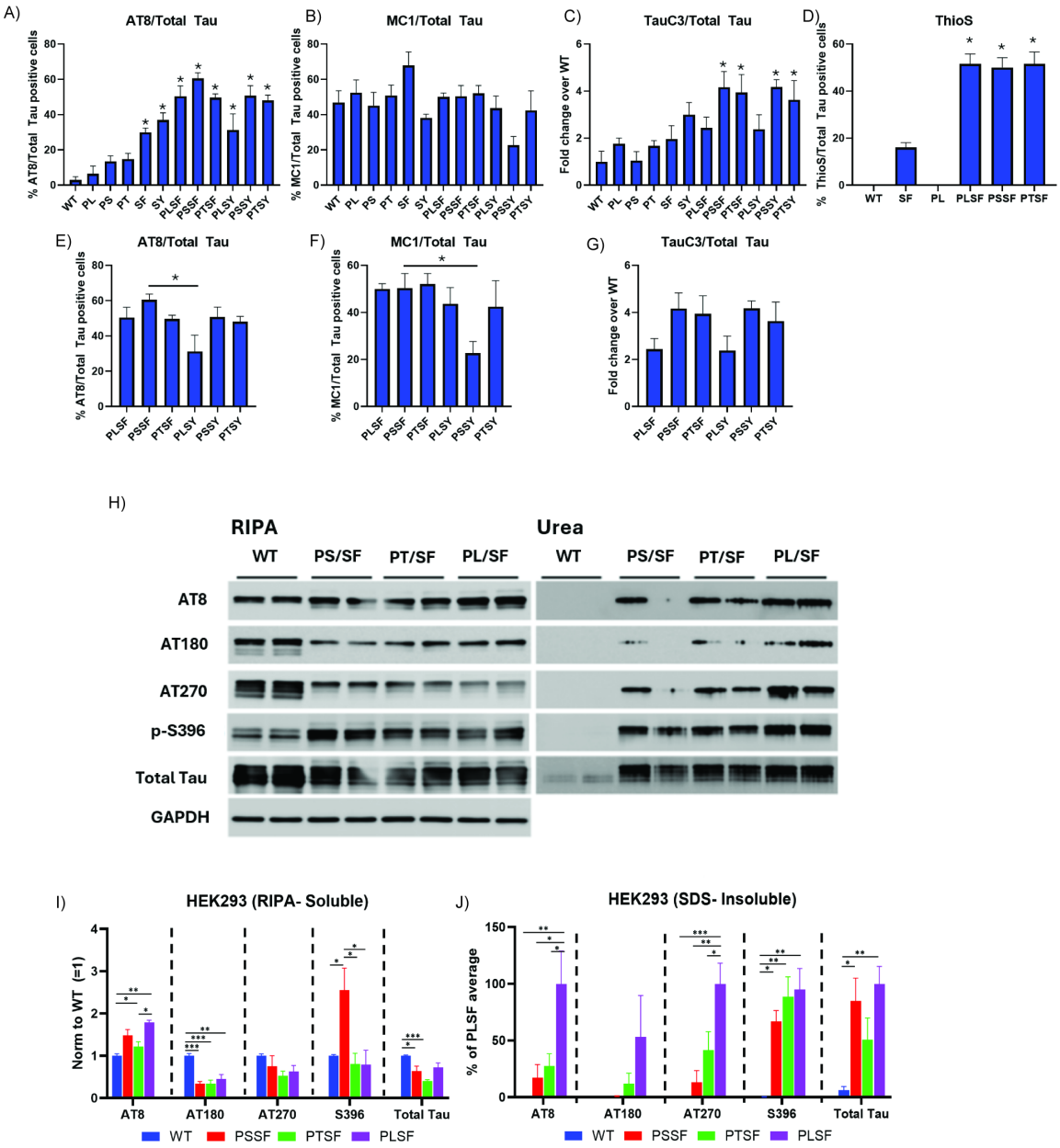

Supplemental Figure 2: Immunoblotting analysis of a panel of P301 and S320 single and combination mutants.

A-G) Quantification of AT8, MC1, TauC3, and ThioS immunocytochemistry in QBI-293 cells expressing various P301 and S320 mutants alone or in combination. Panels E-G are subsets of data from A-C to perform additional comparisons among combinatorial mutants. Representative

818 images not shown. Error bars= SEM. *= significant difference by one-way ANOVA. **H)**
819 Representative immunoblots from QBI-293 cells expressing wild-type, P301S/S320F,
820 P301T/S320F, and P301L/S320F tau variants. RIPA (soluble) and urea (insoluble) fractions were
821 analyzed by immunoblotting for p-tau epitopes (AT8, AT180, AT270, p-396) and total tau (rabbit
822 polyclonal). **I, J)** Quantification of RIPA soluble and urea (insoluble) fractions. Error bars= SEM.
823 *= significant difference by one-way ANOVA.
824
825
826
827
828
829

Bryan et al., Supplemental Figure 3.

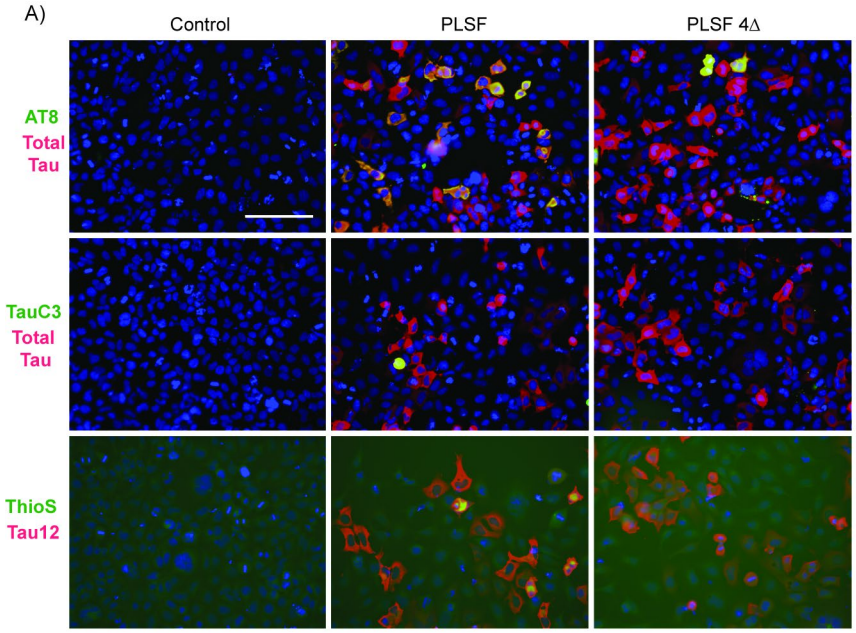

Supplemental Figure 3: Abrogating Hsp binding via the PL-SF 4Δ variant suppresses the accumulation of pathological tau.

Representative immunocytochemistry images from QBI-293 cells expressing tau PL-SF and PL-SF 4Δ tau variants. Cells were probed with AT8 (p-tau), TauC3 (C-terminal cleaved tau) with rabbit polyclonal tau (total tau), and ThioS with Tau12 (human tau). Quantification of images is found in Figure 1F. Control= empty plasmid vector (pcDNA3.1)**.** Scale bar= 125 µm.

Bryan et al., Supplemental Figure 4.

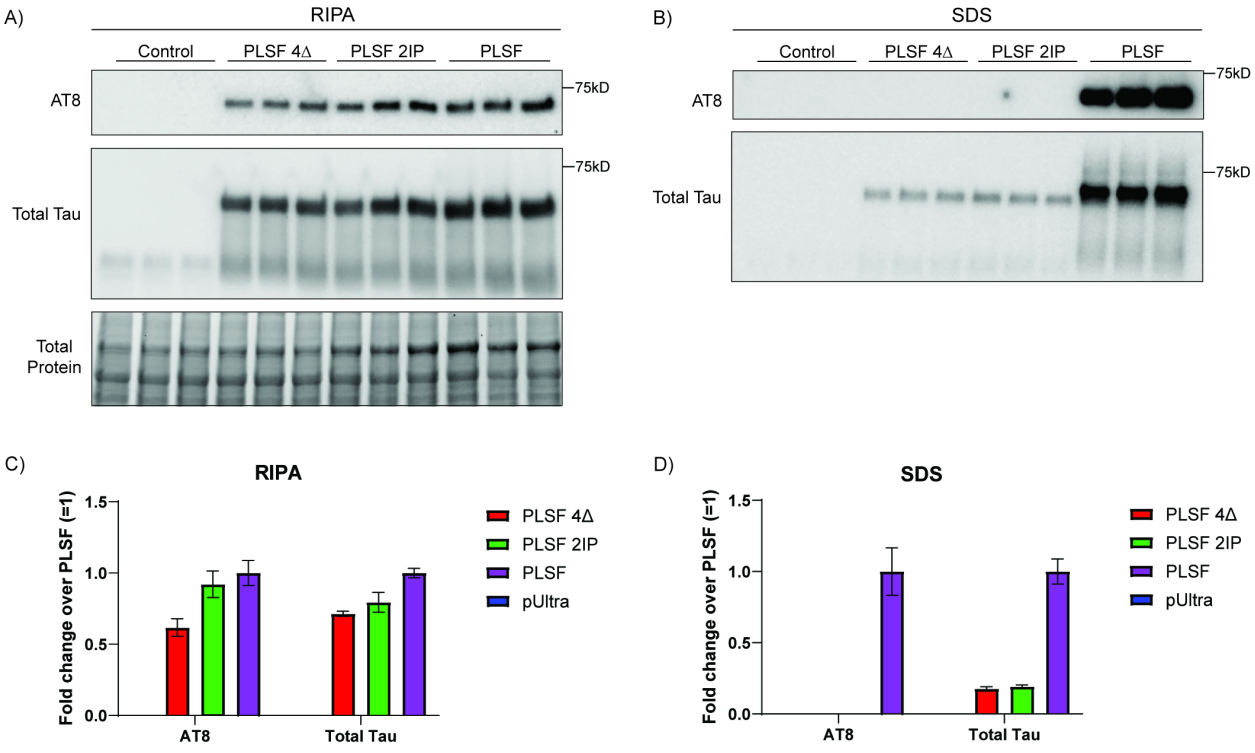

Supplemental Figure 4: PLSF containing the β-structure breaking mutations, I277P/I308P, prevents tau aggregation similar to PLSF 4Δ.

A) Representative RIPA immunoblot of primary neurons transduced with empty control, PLSF 4Δ-eGFP, PLSF I277P/I308P (2IP), or PLSF-eGFP and probed for p-tau (AT8) and total tau (rabbit polyclonal). **B)** Quantification of AT8 and total tau in RIPA fraction. **C)** Representative SDS immunoblot of primary neurons transduced with empty control, PLSF 4Δ-eGFP, PLSF I277P/I308P (2IP), or PLSF-eGFP and probed for p-tau (AT8) and total tau (rabbit polyclonal. **D)** Quantification of SDS fraction. *= significant difference by one-way ANOVA.

Bryan et al., Supplemental Figure 5.

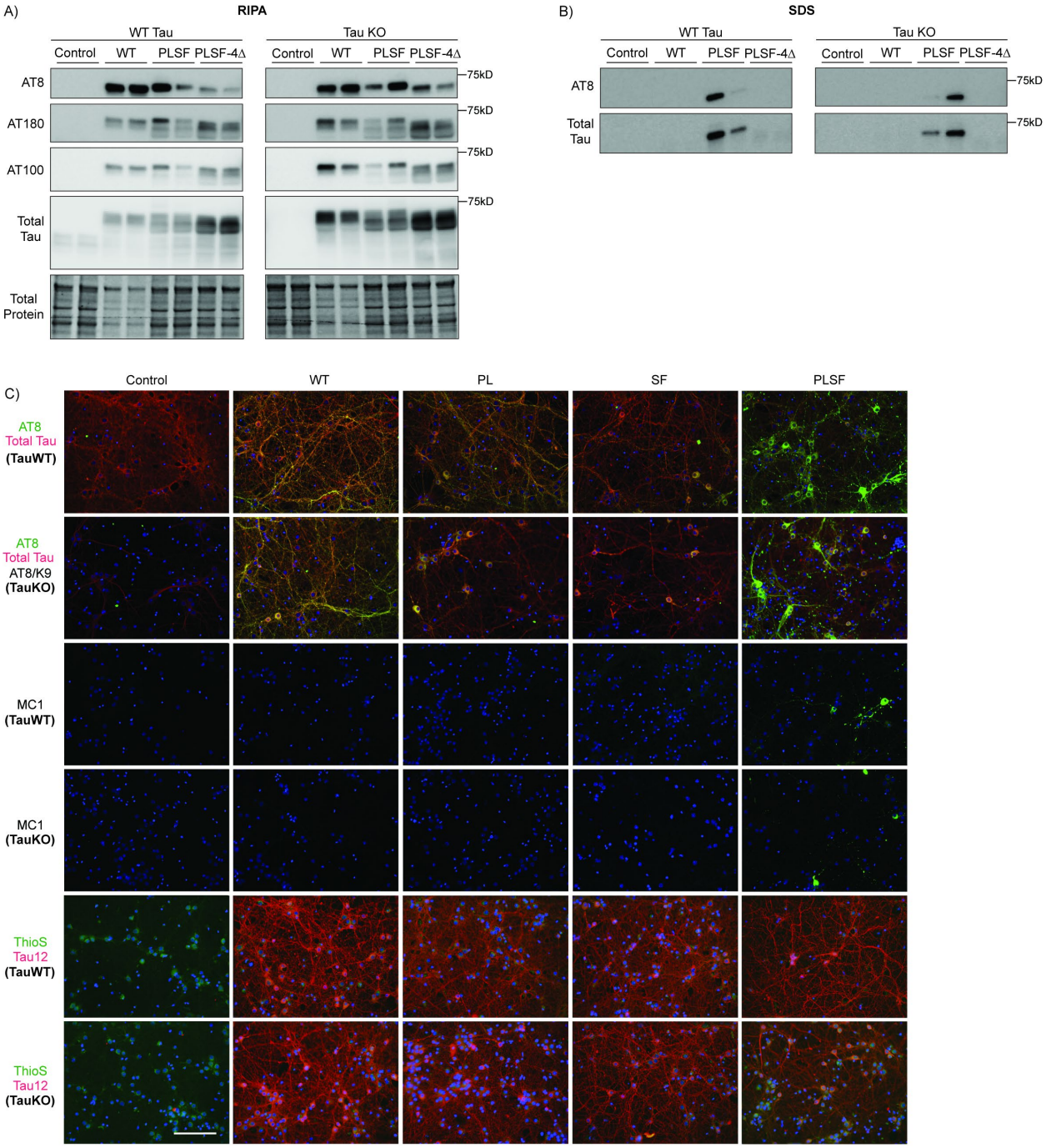

Supplemental Figure 5: PL-SF aggregates emerge similarly in either wild-type or tau knockout neurons lacking endogenous mouse tau.

A) RIPA (soluble) immunoblot of wild-type tau and tau knockout neurons probed with p-tau (AT8, AT180, AT100) and total tau (rabbit polyclonal). **B)** SDS (insoluble) immunoblot of wild-

type tau and tau knockout neurons probed with p-tau (AT8) and total tau (rabbit polyclonal). **C)** Representative immunoblotting images of wild-type, P301L, S320F, and P301L/S320F tau variants in wild-tau-expressing or tau knockout neurons. Neurons were labeled with AT8 (GFP) and rabbit polyclonal total tau (RFP), MC1 (GFP), or ThioS (GFP) and Tau12 (RFP). Scale bar= 125 µm. Control= empty viral vector (pUltra)**.**

Bryan et al., Supplemental Figure 6.

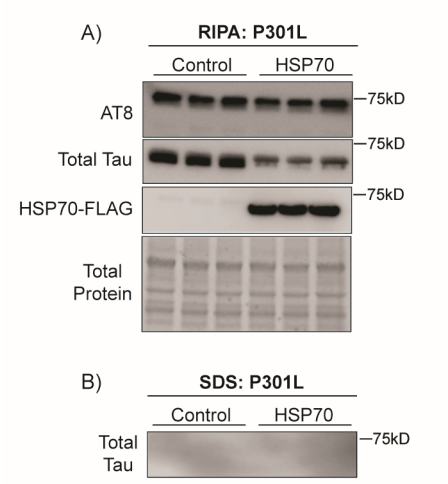

867

868 **Supplemental Figure 6: Overexpression of HSP70 in P301L-expressing neurons does not**
869 **promote tau phosphorylation or aggregation.**

870 **A)** RIPA (soluble) immunoblot of primary neurons following 1-week of lentiviral co-transduction
871 with P301L tau and HSP70. Blot was probed with p-tau (AT8), total tau (rabbit polyclonal), and
872 M2 FLAG (Hsp70-FLAG). **B)** SDS (insoluble) immunoblot of primary neurons was unable to
873 detect insoluble tau species with total tau antibody (rabbit polyclonal). Control= empty viral vector
874 (pUltra)**.**

875

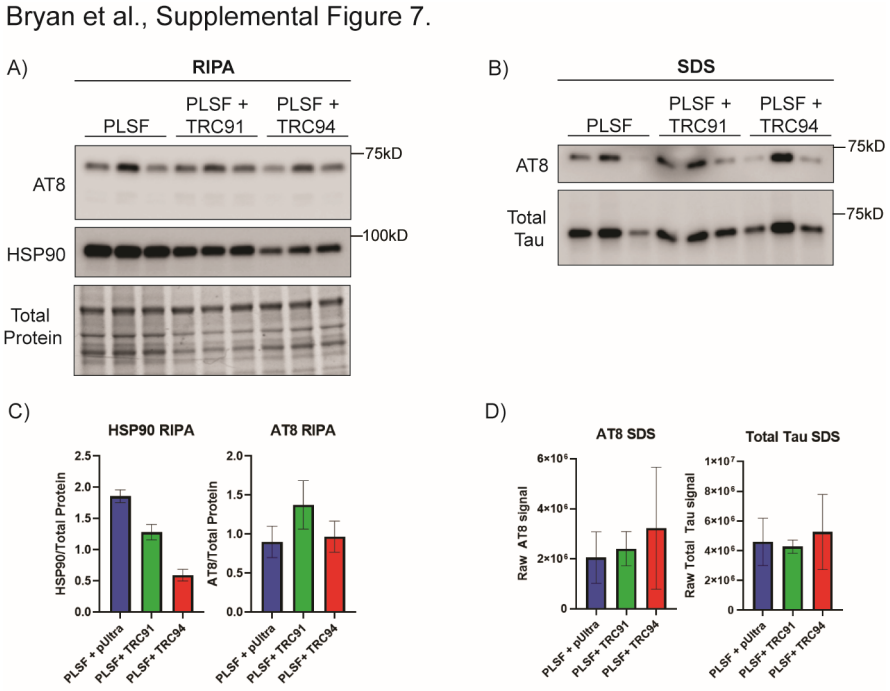

Supplemental Figure 7: HSP90 depletion does not alter phosphorylated or aggregated PL-SF tau.

A) RIPA (soluble) immunoblot of primary neurons probed with p-tau (AT8) and Hsp90 following 1-week of lentiviral HSP90 knockdown with two shRNAs (called TRC91 and TRC94). **B)** SDS (insoluble) immunoblot of primary neurons probed with p-tau (AT8) and total tau (rabbit polyclonal) following 1-week of lentiviral HSP90 knockdown. **C)** Quantification of AT8 and Hsp90 in the RIPA fraction. Error bars= SEM. **D)** Quantification of AT8 and total tau (rabbit polyclonal) in SDS fraction. *Note: Only TRC94, and not TRC91, HSP90 shRNA was able to reduce Hsp90 expression.

Bryan et al., Supplemental Figure 8.

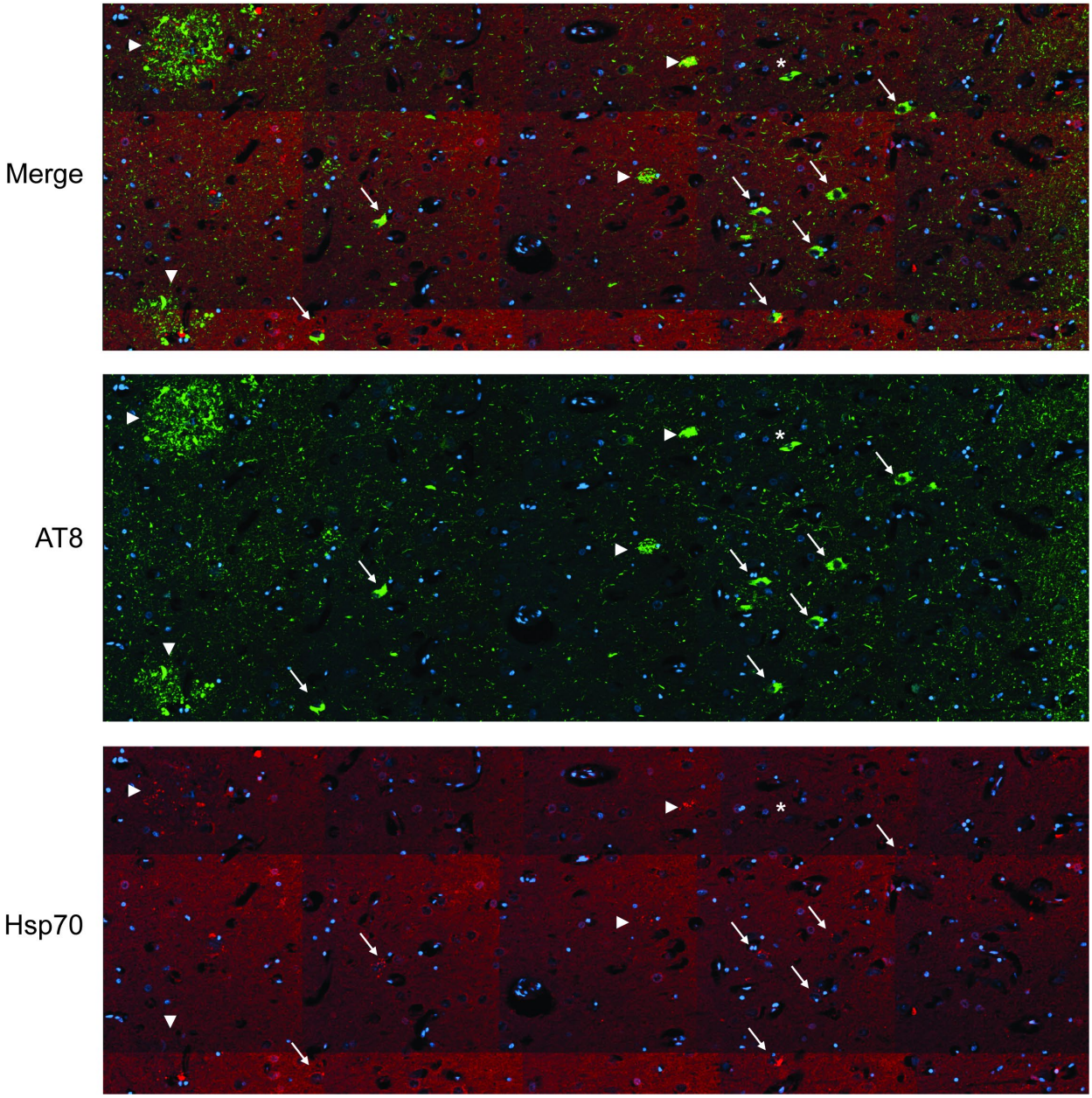

886

887 **Supplemental Figure 8: Hsp70 foci accumulation within neuritic plaques and neurofibrillary**

888 **tangles in human AD brain**

889 **A)** Representative stitched widefield images of a human AD patient hippocampus labeled with

890 AT8 (GFP) and Hsp70 (RFP). AT8/Hsp70 positive plaques are labeled with white arrowheads.

891 AT8/Hsp70 positive tangles are labeled with white arrows. * = a single AT8 positive tangle that is

absent for Hsp70 foci.

Table 1: Primers used for vector construction

Primer	Sequence
d277-278F	AATAAGAAGCTGGATCTTAGCAACGTC
d277-278R	CTGCACCTTCCCGCCTCC
d308-309F	TACAAACCAGTTGACCTGAGCAAG
d308-309R	TTGCACACTGCCGCCTCC
Tau F	CCGACCGGTGCCACCATGGCTGAGCCCCGCCAG
Tau R	CGCGTCGACTCACAAACCCTGCTTGGCCAGG
I308P-F	CAGTGTGCAAccgGTCTACAAACCAGTTGACCTGAGcaagg
I308P-R	CCGCCTCCCAGGACGtgtttg
I277P-F	GAAGGTGCAGccgATTAATAAGAAGCTGGATCTTAGCAACGtccagtcc
HSP70-F	GCGACCGGTGCCACCATGGATTACAAGGATGACGACGATAAGATGGCCAAAGCCGCGGCGATCG
HSP70-R	TCGGTCGACCTAATCTACCTCCTCAATGGTGGGGCC
HSC70-F	GCGACCGGTGCCACCATGGATTACAAGGATGACGACGATAAGATGTCCAAGGGACCTGCAGTTGG
HSC70-R	TCGGTCGACATCAACCTCTTCAATGGTGGGCCC
Hsp90-F	GCGACCGGTGCCACCATGGATTACAAGGATGACGACGATAAG
Hsp90-R	GCGGTCGACGCTAGTCTACTTCTTCCATGCGTGATGTG

921 **References**
922
923

924 1. Strang, K. H., Golde, T. E. & Giasson, B. I. MAPT mutations, tauopathy, and mechanisms of
925 neurodegeneration. *Lab. Investig.* **99**, 912–928 (2019).

926 2. Sanders, D. W. *et al.* Distinct tau prion strains propagate in cells and mice and define different
927 tauopathies. *Neuron* **82**, 1271–88 (2014).

928 3. Peeraer, E. *et al.* Intracerebral injection of preformed synthetic tau fibrils initiates widespread
929 tauopathy and neuronal loss in the brains of tau transgenic mice. *Neurobiol. Dis.* **73**, 83–95
930 (2015).

931 4. Clavaguera, F. *et al.* Transmission and spreading of tauopathy in transgenic mouse brain. *Nat.*
932 *Cell Biol.* **11**, 909–913 (2009).

933 5. Chen, D. *et al.* FTD-tau S320F mutation stabilizes local structure and allosterically promotes
934 amyloid motif-dependent aggregation. *Nat. Commun.* **14**, 1625 (2023).

935 6. Rosso, S. M. *et al.* A noveltau mutation, S320F, causes a tauopathy with inclusions similar to
936 those in Pick's disease. *Ann Neurol* **51**, 373–376 (2002).

937 7. Trzeciakiewicz, H. *et al.* An HDAC6-dependent surveillance mechanism suppresses tau-
938 mediated neurodegeneration and cognitive decline. *Nat Commun* **11**, 5522 (2020).

939 8. Koller, E. J. *et al.* Combining P301L and S320F tau variants produces a novel accelerated
940 model of tauopathy. *Hum Mol Genet* **28**, 3255–3269 (2019).

941 9. Strang, K. H. *et al.* Distinct differences in prion-like seeding and aggregation between tau
942 protein variants provide mechanistic insights into tauopathies. *J Biological Chem* **293**, 2408–
943 2421 (2017).

944 10. Croft, C. L. *et al.* rAAV-based brain slice culture models of Alzheimer's and Parkinson's
945 disease inclusion pathologies. *J Exp Medicine* **216**, 539–555 (2019).

946 11. Xia, Y. *et al.* Pathogenic tau recruits wild-type tau into brain inclusions and induces gut
947 degeneration in transgenic SPAM mice. *Commun Biology* **5**, 446 (2022).

948 12. Beckman, D. *et al.* Temporal progression of tau pathology and neuroinflammation in a rhesus
949 monkey model of Alzheimer's disease. *Alzheimer's Dement.* **20**, 5198–5219 (2024).

950 13. Kaniyappan, S. *et al.* FRET-based Tau seeding assay does not represent prion-like templated
951 assembly of Tau filaments. *Mol. Neurodegener.* **15**, 39 (2020).

952 14. Smith, E. D. *et al.* Tau from SPAM Transgenic Mice Exhibit Potent Strain-Specific Prion-
953 Like Seeding Properties Characteristic of Human Neurodegenerative Diseases. *NeuroMolecular*
954 *Med.* **27**, 44 (2025).

955 15. Croft, C. L. *et al.* Photodynamic studies reveal rapid formation and appreciable turnover of
956 tau inclusions. *Acta Neuropathol* 1–23 (2021) doi:10.1007/s00401-021-02264-9.

957 16. Jinwal, U. K. *et al.* Imbalance of Hsp70 family variants fosters tau accumulation. *FASEB J.*
958 **27**, 1450–1459 (2013).

959 17. Voss, K., Combs, B., Patterson, K. R., Binder, L. I. & Gamblin, T. C. Hsp70 Alters Tau
960 Function and Aggregation in an Isoform Specific Manner. *Biochemistry* **51**, 888–898 (2012).

961 18. Jinwal, U. K. *et al.* Hsc70 Rapidly Engages Tau after Microtubule Destabilization*. *J Biol*
962 *Chem* **285**, 16798–16805 (2010).

963 19. Rutledge, B. S., Choy, W.-Y. & Duennwald, M. L. Folding or holding?—Hsp70 and Hsp90
964 chaperoning of misfolded proteins in neurodegenerative disease. *J. Biol. Chem.* **298**, 101905
965 (2022).

966 20. Petrucelli, L. *et al.* CHIP and Hsp70 regulate tau ubiquitination, degradation and aggregation.
967 *Hum Mol Genet* **13**, 703–714 (2004).

968 21. Thompson, A. D. *et al.* Analysis of the Tau-Associated Proteome Reveals That Exchange of
969 Hsp70 for Hsp90 Is Involved in Tau Degradation. *ACS Chem. Biol.* **7**, 1677–1686 (2012).

970 22. Fontaine, S. N. *et al.* Isoform-selective Genetic Inhibition of Constitutive Cytosolic Hsp70
971 Activity Promotes Client Tau Degradation Using an Altered Co-chaperone Complement*. *J Biol*
972 *Chem* **290**, 13115–13127 (2015).

973 23. Young, Z. T. *et al.* Stabilizing the Hsp70-Tau Complex Promotes Turnover in Models of
974 Tauopathy. *Cell Chem. Biol.* **23**, 992–1001 (2016).

975 24. Pratt, W. B., Gestwicki, J. E., Osawa, Y. & Lieberman, A. P. Targeting Hsp90/Hsp70-Based
976 Protein Quality Control for Treatment of Adult Onset Neurodegenerative Diseases. *Annu. Rev.*
977 *Pharmacol. Toxicol.* **55**, 353–371 (2015).

978 25. Dickey, C. A. *et al.* The high-affinity HSP90-CHIP complex recognizes and selectively
979 degrades phosphorylated tau client proteins. *J Clin Invest* **117**, 648–658 (2007).

980 26. Xu, P. *et al.* Allosteric inhibition of HSP70 in collaboration with STUB1 augments
981 enzalutamide efficacy in antiandrogen resistant prostate tumor and patient-derived models.
982 *Pharmacol. Res.* **189**, 106692 (2023).

983 27. Li, X. *et al.* Analogues of the Allosteric Heat Shock Protein 70 (Hsp70) Inhibitor, MKT-077,
984 As Anti-Cancer Agents. *Acs Med Chem Lett* **4**, 1042–1047 (2013).

985 28. Miyata, Y. *et al.* Synthesis and Initial Evaluation of YM-08, a Blood-Brain Barrier
986 Permeable Derivative of the Heat Shock Protein 70 (Hsp70) Inhibitor MKT-077, Which Reduces
987 Tau Levels. *Acs Chem Neurosci* **4**, 930–939 (2013).

988 29. Moradi-Marjaneh, R., Paseban, M. & Marjaneh, M. M. Hsp70 inhibitors: Implications for the
989 treatment of colorectal cancer. *IUBMB Life* **71**, 1834–1845 (2019).

990 30. Abisambra, J. *et al.* Allosteric Heat Shock Protein 70 Inhibitors Rapidly Rescue Synaptic
991 Plasticity Deficits by Reducing Aberrant Tau. *Biol Psychiat* **74**, 367–374 (2013).

992 31. Biamonte, M. A. *et al.* Heat Shock Protein 90: Inhibitors in Clinical Trials. *J. Med. Chem.*
993 **53**, 3–17 (2010).

994 32. Kundel, F. *et al.* Hsp70 Inhibits the Nucleation and Elongation of Tau and Sequesters Tau
995 Aggregates with High Affinity. *ACS Chem. Biol.* **13**, 636–646 (2018).

996 33. Patterson, K. R. *et al.* Heat Shock Protein 70 Prevents both Tau Aggregation and the
997 Inhibitory Effects of Preexisting Tau Aggregates on Fast Axonal Transport. *Biochemistry* **50**,
998 10300–10310 (2011).

999 34. Fontaine, S. N. *et al.* DnaJ/Hsc70 chaperone complexes control the extracellular release of
1000 neurodegenerative-associated proteins. *EMBO J.* **35**, 1537–1549 (2016).

1001 35. Abisambra, J. F. *et al.* DnaJA1 Antagonizes Constitutive Hsp70-Mediated Stabilization of
1002 Tau. *J. Mol. Biol.* **421**, 653–661 (2012).

1003 36. Sarkar, M., Kuret, J. & Lee, G. Two motifs within the tau microtubule-binding domain
1004 mediate its association with the hsc70 molecular chaperone. *J Neurosci Res* **86**, 2763–2773
1005 (2008).

1006 37. Joseph, M., Anglada-Huguet, M., Paesler, K., Mandelkow, E. & Mandelkow, E.-M. Anti-
1007 aggregant tau mutant promotes neurogenesis. *Mol Neurodegener* **12**, 88 (2017).

1008 38. Pir, G. J. *et al.* Suppressing Tau Aggregation and Toxicity by an Anti-Aggregant Tau
1009 Fragment. *Mol Neurobiol* **56**, 3751–3767 (2019).

1010 39. Sydow, A. *et al.* Tau-Induced Defects in Synaptic Plasticity, Learning, and Memory Are
1011 Reversible in Transgenic Mice after Switching Off the Toxic Tau Mutant. *J Neurosci* **31**, 2511–
1012 2525 (2011).

1013 40. Mocanu, M.-M. *et al.* The Potential for -Structure in the Repeat Domain of Tau Protein
1014 Determines Aggregation, Synaptic Decay, Neuronal Loss, and Coassembly with Endogenous
1015 Tau in Inducible Mouse Models of Tauopathy. *J Neurosci* **28**, 737–748 (2008).

1016 41. Bergen, M. von *et al.* Mutations of Tau Protein in Frontotemporal Dementia Promote
1017 Aggregation of Paired Helical Filaments by Enhancing Local β-Structure. *J Biol Chem* **276**,
1018 48165–48174 (2001).

1019 42. Morito, T. *et al.* Human MAPT knockin mouse models of frontotemporal dementia for the
1020 neurodegenerative research community. *Cell Rep. Methods* **5**, 101024 (2025).

1021 43. Beckman, D. *et al.* A novel tau-based rhesus monkey model of Alzheimer's pathogenesis.
1022 *Alzheimer's Dement.* **17**, 933–945 (2021).

1023 44. Scheres, S. H., Zhang, W., Falcon, B. & Goedert, M. Cryo-EM structures of tau filaments.
1024 *Curr. Opin. Struct. Biol.* **64**, 17–25 (2020).

1025 45. Fitzpatrick, A. W. P. *et al.* Cryo-EM structures of tau filaments from Alzheimer's disease.
1026 *Nature* **547**, 185–190 (2017).

1027 46. Tarutani, A. *et al.* Cryo-EM structures of tau filaments from SH-SY5Y cells seeded with
1028 brain extracts from cases of Alzheimer's disease and corticobasal degeneration. *FEBS Open Bio*
1029 **13**, 1394–1404 (2023).

1030 47. Arakhamia, T. *et al.* Posttranslational Modifications Mediate the Structural Diversity of
1031 Tauopathy Strains. *Cell* (2020) doi:10.1016/j.cell.2020.01.027.

1032 48. Schweighauser, M. *et al.* Cryo-EM structures of tau filaments from the brains of mice
1033 transgenic for human mutant P301S Tau. *Acta Neuropathol. Commun.* **11**, 160 (2023).

1034 49. Zhao, W. *et al.* Cryo-EM structures reveal variant Tau amyloid fibrils between the rTg4510
1035 mouse model and sporadic human tauopathies. *Cell Discov.* **10**, 27 (2024).

1036 50. Nixon, R. A. Autophagy–lysosomal-associated neuronal death in neurodegenerative disease.
1037 *Acta Neuropathol.* **148**, 42 (2024).

1038 51. Ihara, Y., Morishima-Kawashima, M. & Nixon, R. The Ubiquitin–Proteasome System and
1039 the Autophagic–Lysosomal System in Alzheimer Disease. *Cold Spring Harb. Perspect. Med.* **2**,
1040 a006361 (2012).

1041 52. Keller, J. N., Hanni, K. B. & Markesbery, W. R. Impaired Proteasome Function in
1042 Alzheimer's Disease. *J. Neurochem.* **75**, 436–439 (2000).

1043 53. Bobkova, N. V. *et al.* Therapeutic Effect of Exogenous Hsp70 in Mouse Models of
1044 Alzheimer's Disease. *J. Alzheimer's Dis.* **38**, 425–435 (2014).

1045 54. Nachman, E. *et al.* Disassembly of Tau fibrils by the human Hsp70 disaggregation machinery
1046 generates small seeding-competent species. *J Biol Chem* **295**, 9676–9690 (2020).

1047 55. Fontaine, S. N. *et al.* The active Hsc70/tau complex can be exploited to enhance tau turnover
1048 without damaging microtubule dynamics. *Hum Mol Genet* **24**, 3971–3981 (2015).

1049 56. Yang, X. & Tohda, C. Heat Shock Cognate 70 Inhibitor, VER-155008, Reduces Memory
1050 Deficits and Axonal Degeneration in a Mouse Model of Alzheimer's Disease. *Front. Pharmacol.*
1051 **9**, 48 (2018).

1052 57. Jinwal, U. K. *et al.* Chemical Manipulation of Hsp70 ATPase Activity Regulates Tau
1053 Stability. *J Neurosci* **29**, 12079–12088 (2009).

1054 58. Yu, A. *et al.* Tau protein aggregates inhibit the protein-folding and vesicular trafficking arms
1055 of the cellular proteostasis network. *J Biol Chem* **294**, 7917–7930 (2019).

1056 59. Dou, F. *et al.* Chaperones increase association of tau protein with microtubules. *Proc*
1057 *National Acad Sci* **100**, 721–726 (2003).

1058 60. Vries, L. E. de *et al.* Gene-expression profiling of individuals resilient to Alzheimer's disease
1059 reveals higher expression of genes related to metallothionein and mitochondrial processes and no
1060 changes in the unfolded protein response. *Acta Neuropathol. Commun.* **12**, 68 (2024).

1061 61. Hondius, D. C. *et al.* The proteome of granulovacuolar degeneration and neurofibrillary
1062 tangles in Alzheimer's disease. *Acta Neuropathol.* **141**, 341–358 (2021).

1063 62. Salminen, A., Ojala, J., Kaarniranta, K., Hiltunen, M. & Soininen, H. Hsp90 regulates tau
1064 pathology through co-chaperone complexes in Alzheimer's disease. *Prog Neurobiol* **93**, 99–110
1065 (2011).

1066 63. Moll, A. *et al.* Hsp multichaperone complex buffers pathologically modified Tau. *Nat*
1067 *Commun* **13**, 3668 (2022).

1068 64. Karagöz, G. E. *et al.* Hsp90-Tau Complex Reveals Molecular Basis for Specificity in
1069 Chaperone Action. *Cell* **156**, 963–974 (2014).

1070 65. Cook, C. *et al.* Loss of HDAC6, a novel CHIP substrate, alleviates abnormal tau
1071 accumulation. *Hum Mol Genet* **21**, 2936–45 (2012).

1072 66. Dickey, C. A. *et al.* Akt and CHIP coregulate tau degradation through coordinated
1073 interactions. *P Natl Acad Sci Usa* **105**, 3622–7 (2008).

1074 67. Weickert, S., Wawrzyniuk, M., John, L. H., Rüdiger, S. G. D. & Drescher, M. The
1075 mechanism of Hsp90-induced oligomerizaton of Tau. *Sci Adv* **6**, eaax6999 (2020).

1076 68. Miyata, Y. *et al.* Cysteine Reactivity Distinguishes Redox Sensing by the Heat-Inducible and
1077 Constitutive Forms of Heat Shock Protein 70. *Chem. Biol.* **19**, 1391–1399 (2012).

1078 69. Shelton, L. B. *et al.* Hsp90 activator Aha1 drives production of pathological tau aggregates.
1079 *Proc National Acad Sci* **114**, 9707–9712 (2017).

1080 70. Jinwal, U. K. *et al.* The Hsp90 Cochaperone, FKBP51, Increases Tau Stability and
1081 Polymerizes Microtubules. *J. Neurosci.* **30**, 591–599 (2010).

1082 71. Blair, L. J. *et al.* Accelerated neurodegeneration through chaperone-mediated
1083 oligomerization of tau. *J. Clin. Investig.* **123**, 4158–4169 (2013).

1084 72. Webster, J. M. *et al.* Hsp22 with an N-Terminal Domain Truncation Mediates a Reduction in
1085 Tau Protein Levels. *Int. J. Mol. Sci.* **21**, 5442 (2020).

1086 73. Ospina, S. R. *et al.* Small Heat Shock Protein 22 Improves Cognition and Learning in the
1087 Tauopathic Brain. *Int J Mol Sci* **23**, 851 (2022).

1088 74. Abisambra, J. F. *et al.* Phosphorylation Dynamics Regulate Hsp27-Mediated Rescue of
1089 Neuronal Plasticity Deficits in Tau Transgenic Mice. *J. Neurosci.* **30**, 15374–15382 (2010).

1090 75. Barghorn, S., Biernat, J. & Mandelkow, E. Amyloid Proteins, Methods and Protocols.
1091 *Methods Mol. Biol. (Clifton, NJ)* **299**, 35–51 (2004).

1092 76. Farizatto, K. L. G., Almeida, M. F., Long, R. T. & Bahr, B. A. Early Synaptic Alterations
1093 and Selective Adhesion Signaling in Hippocampal Dendritic Zones Following Organophosphate
1094 Exposure. *Sci. Rep.* **9**, 6532 (2019).

1095 77. Almeida, M. F. *et al.* Distinct and dementia-related synaptopathy in the hippocampus after
1096 military blast exposures. *Brain Pathol.* **31**, e12936 (2021).

1097 78. McKenna, M. *et al.* Organotypic whole hemisphere brain slice models to study the effects of
1098 donor age and oxygen-glucose-deprivation on the extracellular properties of cortical and striatal
1099 tissue. *J. Biol. Eng.* **16**, 14 (2022).

1100 79. Bahr, B. A. *et al.* Amyloid β protein is internalized selectively by hippocampal field CA1 and
1101 causes neurons to accumulate amyloidogenic carboxyterminal fragments of the amyloid
1102 precursor protein. *J. Comp. Neurol.* **397**, 139–147 (1998).

1103 80. Caba, E. *et al.* Excitotoxic stimulation activates distinct pathogenic and protective expression
1104 signatures in the hippocampus. *J. Cell. Mol. Med.* **25**, 9011–9027 (2021).

1105 81. Farizatto, K. L. G., Ikonne, U. S., Almeida, M. F., Ferrari, M. F. R. & Bahr, B. A. Aβ42-
1106 mediated proteasome inhibition and associated tau pathology in hippocampus are governed by a
1107 lysosomal response involving cathepsin B: Evidence for protective crosstalk between protein
1108 clearance pathways. *PLoS ONE* **12**, e0182895 (2017).

1109